

RESEARCH ARTICLE

Bruton Tyrosine Kinase–Dependent Immune Cell Cross-talk Drives Pancreas Cancer

Andrew J. Gunderson¹, Megan M. Kaneda², Takahiro Tsujikawa^{1,3}, Abraham V. Nguyen², Nesrine I. Affara⁴, Brian Ruffell¹, Sara Gorjestani², Shannon M. Liudahl¹, Morgan Truitt⁵, Peter Olson⁵, Grace Kim^{4,6}, Douglas Hanahan⁷, Margaret A. Tempero^{6,8}, Brett Sheppard^{9,10}, Bryan Irving¹¹, Betty Y. Chang¹², Judith A. Varner^{2,13}, and Lisa M. Coussens^{1,10}

ABSTRACT

Pancreas ductal adenocarcinoma (PDAC) has one of the worst 5-year survival rates of all solid tumors, and thus new treatment strategies are urgently needed. Here, we report that targeting Bruton tyrosine kinase (BTK), a key B-cell and macrophage kinase, restores T cell–dependent antitumor immune responses, thereby inhibiting PDAC growth and improving responsiveness to standard-of-care chemotherapy. We report that PDAC tumor growth depends on cross-talk between B cells and FcR γ tumor-associated macrophages, resulting in T_H2-type macrophage programming via BTK activation in a PI3K γ -dependent manner. Treatment of PDAC-bearing mice with the BTK inhibitor PCI32765 (ibrutinib) or by PI3K γ inhibition reprogrammed macrophages toward a T_H1 phenotype that fostered CD8⁺ T-cell cytotoxicity, and suppressed PDAC growth, indicating that BTK signaling mediates PDAC immunosuppression. These data indicate that pharmacologic inhibition of BTK in PDAC can reactivate adaptive immune responses, presenting a new therapeutic modality for this devastating tumor type.

SIGNIFICANCE: We report that BTK regulates B-cell and macrophage-mediated T-cell suppression in pancreas adenocarcinomas. Inhibition of BTK with the FDA-approved inhibitor ibrutinib restores T cell–dependent antitumor immune responses to inhibit PDAC growth and improves responsiveness to chemotherapy, presenting a new therapeutic modality for pancreas cancer. *Cancer Discov*; 6(3): 270–85. ©2015 AACR.

See related commentary by Roghanian et al., p. 230.

See related article by Pylayeva-Gupta et al., p. 247.

See related article by Lee et al., p. 256.

¹Department of Cell, Developmental and Cancer Biology, Oregon Health and Science University, Portland, Oregon. ²Moore's Cancer Center, University of California, San Diego, La Jolla, California. ³Department of Otolaryngology-Head and Neck Surgery, Oregon Health and Science University, Portland, Oregon. ⁴Department of Pathology, University of California, San Francisco, California. ⁵Department of Biochemistry and Biophysics, University of California, San Francisco, California. ⁶Helen Diller Family Comprehensive Cancer Center, University of California, San Francisco, California. ⁷Swiss Institute for Experimental Cancer Research, Swiss Federal Institute of Technology, Lausanne, Switzerland. ⁸Department of Medicine, University of California, San Francisco, California. ⁹Department of Surgery, Oregon Health and Science University, Portland, Oregon. ¹⁰Knight Cancer Institute, Oregon Health and Science University, Portland, Oregon. ¹¹Genentech, South San Francisco, California. ¹²Pharmacyclics Inc., Sunnyvale, California. ¹³Department of Pathology, University of California, San Diego, La Jolla, California.

Note: Supplementary data for this article are available at Cancer Discovery Online (<http://cancerdiscovery.aacrjournals.org/>).

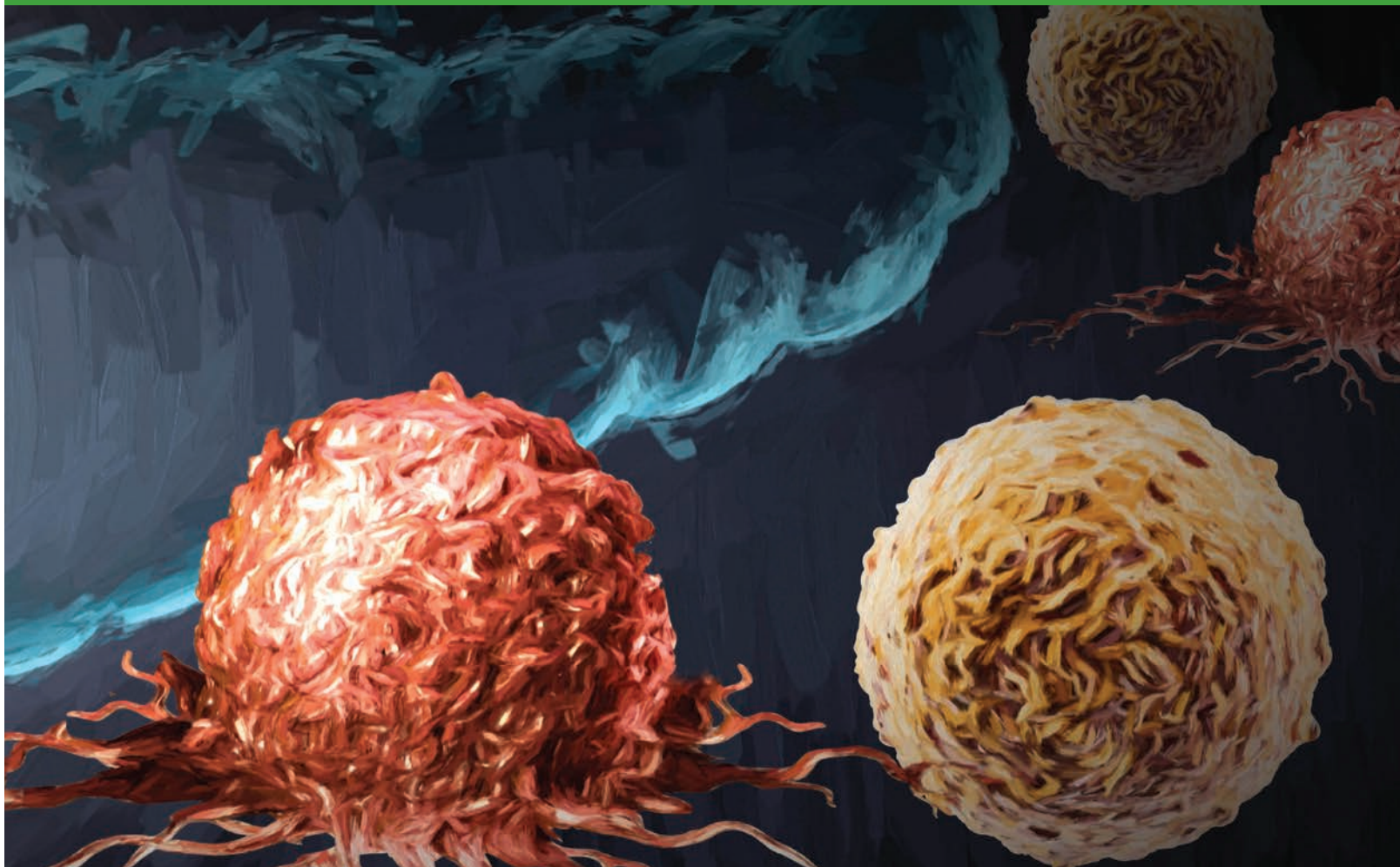
A.J. Gunderson, M.M. Kaneda, J.A. Varner, and L.M. Coussens contributed equally to this article.

Current address for B. Irving: CytomX Therapeutics Inc., South San Francisco, CA.

Corresponding Authors: Lisa M. Coussens, Cell, Developmental and Cancer Biology, Knight Cancer Institute, Oregon Health and Science University, 181 SW Sam Jackson Park Road, Code 1215, Portland, OR 97239-3098. Phone: 503-494-7811; Fax: 503-494-4253; E-mail: cousseni@ohsu.edu; and Judith A. Varner, Department of Pathology, Moore's Cancer Center, University of California, San Diego, 3855 Health Sciences Drive, La Jolla, CA 92093-0819. Phone: 858-822-0086; Fax: 858-822-1325; E-mail: jvarner@ucsd.edu

doi: 10.1158/2159-8290.CD-15-0827

©2015 American Association for Cancer Research.



INTRODUCTION

The contribution of tissue-resident and recruited leukocytes to the progression of solid tumors is now a widely accepted mechanism of pathogenesis (1, 2), and one that is gaining notable traction in the clinic (3). Although many studies have dissected the numerous activities leukocytes exert toward regulating neoplastic progression, tractable immune-based targets for anticancer therapy are only just emerging.

Ductal adenocarcinoma of the pancreas (PDAC) is a devastating disease with one of the lowest 5-year survival rates of all solid tumors (4). Currently, 7.2% of patients with newly diagnosed pancreatic cancer will survive 5 years following diagnosis, due in part to the fact that PDAC is rarely detected at an early stage; instead, the majority of patients present with locally unresectable or metastatic disease (5). Because standard therapies have only a modest impact on survival (6, 7), novel therapeutic and diagnostic strategies are urgently needed.

A characteristic feature of PDAC tumors is the presence of abundant infiltrating leukocytes representing both lymphoid and myeloid lineages (8); thus, we sought to identify functionally significant immune-based programs regulating pancreatic carcinogenesis that would be tractable for therapeutic

intervention. We report here that B cell–macrophage interactions promote PI3K γ - and Bruton tyrosine kinase (BTK)-dependent macrophage T_H2 polarization, leading to immune suppression and PDAC progression. Using mouse models of PDAC, targeted inhibition of BTK, a common signaling molecule in B cells and myeloid cells, resulted in slowed PDAC tumor growth, abated immune suppression, impeded late-stage tumor growth, and improved responsiveness to standard-of-care chemotherapy (CTX), indicating that targeting BTK therapeutically could provide long-term antitumor control for this devastating malignancy.

RESULTS

B Cells and FcR γ -Positive Cells in Human PDAC

We previously identified a protumorigenic role for CD20⁺ B cells in solid tumors using murine models of squamous cell carcinogenesis, and demonstrated that therapeutic depletion of B cells in squamous cell carcinoma (SCC)-bearing mice resulted in an improved response to CTX by CD8⁺ T cell-dependent mechanisms (9). To identify which human solid tumors might be regulated by protumorigenic B cells, we examined cDNA microarrays of ~3,000 human tumors to assess levels of *CD20* and immunoglobulin (*Ig*) mRNA expression

relative to corresponding normal tissue (9). As expected, human SCCs of the vulva and head and neck exhibited high expression of both mRNAs (9). Human PDACs also exhibited increased *CD20* and *Ig* expression relative to corresponding healthy pancreas tissue, whereas intrapapillary mucinous neoplasias (IPMN) and islet cell carcinomas did not (Fig. 1A). Using an independent data set, we confirmed increased expression of *CD20*, *IgG3*, and *IgM* mRNA in human PDACs (Supplementary Fig. S1A) and correlated with significantly increased plasma IgG in patients with late-stage PDAC (Supplementary Fig. S1B). To quantitatively evaluate the presence of specific leukocyte lineages in healthy pancreata versus regions of resected PDACs, we evaluated fresh single-cell suspensions from surgically resected healthy pancreata and primary human PDAC tumors by polychromatic flow cytometry (FACS; Supplementary Fig. S1C). We found that CD45⁺ leukocyte infiltration of PDAC tumors was significantly increased as compared with healthy pancreas tissue (Fig. 1B), and in PDAC from either chemo-naïve or chemo-treated patients, tumors were dominated by B cells and CD4⁺ and CD8⁺ T cells (Fig. 1C; Supplementary Fig. S1D), similar to reports from other studies (8).

Based on our previous data indicating that B cells regulate protumorigenic programming of Ig receptor gamma (FcγR)-positive myeloid cells (9), we next evaluated publicly available data sets for FcγR expression. We found that *FCGR1*, *FCGR2B*, and *FCGR3B* mRNAs were increased in PDACs as compared with healthy pancreas (Fig. 1D). In addition, we evaluated the frequency of leukocytes expressing CD64 (FcγR1) and CD16 (FcγRIII), the activating forms of FcγR, in human PDAC tumors, and found the highest levels of CD64 on macrophages, dendritic cells (DC), and immature monocytes, and the highest levels of CD16 instead on eosinophils and neutrophils (Fig. 1E). Based on these collective data, we hypothesized that, similar to murine SCCs, B cells cooperate with FcγR-positive myeloid cells to foster PDAC tumorigenesis.

B Cells and FcγR-Positive Myeloid Cells Foster PDAC Tumorigenesis

To test the hypothesis that B cells collaborate with myeloid cells to promote PDAC tumorigenesis, we investigated tumor growth of two syngeneic murine PDAC cell lines derived from primary pancreatic carcinomas of transgenic *Pdx-Cre; LSL-Kras^{G12D}* mice (10–12) harboring null mutations in *p16^{Ink4a}* (Ink4 2.2) or *Trp53* (p53 2.1.1; refs. 13–16). Both cell lines generated PDACs that were histologically similar to PDACs from the transgenic mice from which they were derived (Supplementary Fig. S2A–S2C). PDAC tumors derived from both cell lines also exhibited similar infiltration by CD45⁺ leukocytes as a percentage of viable cells in tumors (Fig. 2A; Supplementary Fig. S2D), as well as significant B-cell infiltration as compared with wild-type (WT) pancreas tissue as revealed by FACS analysis, predominated by IgM^{hi}CD23⁺ transitional 2 cells, IgM^{hi}CD23⁺CD5⁺ B1a cells, IgM^{hi}CD23⁺CD5⁺CD1d^{lo} B1b cells, IgM^{lo}CD23⁺CD5⁺ follicular B cells, IgM^{lo}CD23⁺ memory B cells, and, to a lesser extent, B cells reflecting marginal zone, regulatory, plasma blast, and plasma cells (Fig. 2B; Supplementary Fig. S2E), and/or immunohistochemical analysis (Supplementary Fig. S2A).

To determine if B cells or FcγR-positive myeloid cells imparted a growth advantage to orthotopic PDACs, cell lines were implanted into syngeneic B cell-proficient (JH^{+/+} or ^{+/−}) or B cell-deficient JH^{−/−} mice (Fig. 2B and C). JH^{−/−} mice possess a deletion in the J segment of the Ig heavy-chain locus and thus do not express IgM or IgG, and thus have no mature B cells in bone marrow or periphery due to blocked B-cell differentiation at the large, CD43⁺ precursor stage (17). Tumor cells were also implanted into Ig receptor FcγR-proficient (FcγR^{+/+} or ^{+/+}) and FcγR-deficient (^{−/−}) mice (18), and tumor growth kinetics and characteristics were evaluated longitudinally (Fig. 2C and D; Supplementary Fig. S2B and S2C). PDACs grown in either B cell-deficient or FcγR-deficient mice were significantly smaller than littermate controls (Fig. 2C and D) and exhibited significantly reduced desmoplasia, as determined by alpha smooth muscle actin (αSMA) immunoreactivity (Fig. 2C and D) and Gomori trichrome staining (Supplementary Fig. S2B and S2C).

Similar to human PDAC expression of *FCGR1*, *FCGR2B*, and *FCGR3B* mRNAs (Fig. 1D), we evaluated expression of CD64 FcγRI and CD16/CD32 FcγRII/III by FACS (Supplementary Fig. S2F) and found high-level expression on tumor-infiltrating macrophages and DCs, and to a lesser degree monocytes and neutrophils (Supplementary Fig. S2F). Macrophages, DCs, monocytes, and neutrophils infiltrating Ink4 2.2-derived PDAC tumors grown in FcγR-deficient (*Il4ra*) mice exhibited no expression of either FcγRI or FcγRII/III molecules (Supplementary Fig. S2G). Because we previously reported that FcγR^{−/−} macrophages in SCC tumors have a shifted gene expression profile favoring expression of mRNAs characterizing T_H1 phenotypes (9, 19), we isolated CD45⁺CD11b⁺MHCII⁺F4/80⁺Ly6C[−] macrophages and CD45⁺CD11b⁺MHCII⁺F4/80⁺CD11c⁺ DCs from Ink4 2.2-derived PDAC tumors harvested from FcγR-proficient versus FcγR-deficient mice, and evaluated a panel of characteristic T_H1 (*Il12b*, *Cd40*, *Ccl5*, *Tap2*, *Batf*, *Flt3*, *Ccl7*, *Socs2*) and T_H2 (*Il4ra*, *Arg1*, *Ido1*) mRNAs. We found significant skewing of both cell types toward a T_H1 phenotype in FcγR-deficient mice (Fig. 2E). These data, together with diminished PDAC growth observed in B cell-null JH^{−/−} mice and Ig receptor-null FcγR^{−/−} mice, thus supported the hypothesis that B cells, as well as subsets of myeloid cells, influence PDAC tumor growth.

B Cell and Myeloid Cell Signaling Pathways in PDAC

Based on these findings and our previous data indicating that B cells and tumor-associated macrophages impede cytotoxic T-cell (CTL) activity to regulate solid tumor development (19, 20), we hypothesized that inhibitors of common signaling pathways active in both B cells and infiltrating macrophages, such as BTK or PI3K signaling, might be efficacious against PDAC tumors (Fig. 3A and B). BTK is a member of the TEC family of cytoplasmic protein tyrosine kinases expressed by multiple hematopoietic-lineage cells; in B lymphocytes, BTK is activated by the B cell receptor (BCR) pathway, whereas in macrophages, BTK is activated downstream of FcγR by spleen tyrosine kinase (Syk; refs. 21, 22). Thus, we examined human PDAC specimens for the presence of BTK⁺ cells in tissue sections and found BTK immunoreactivity in CD45⁺

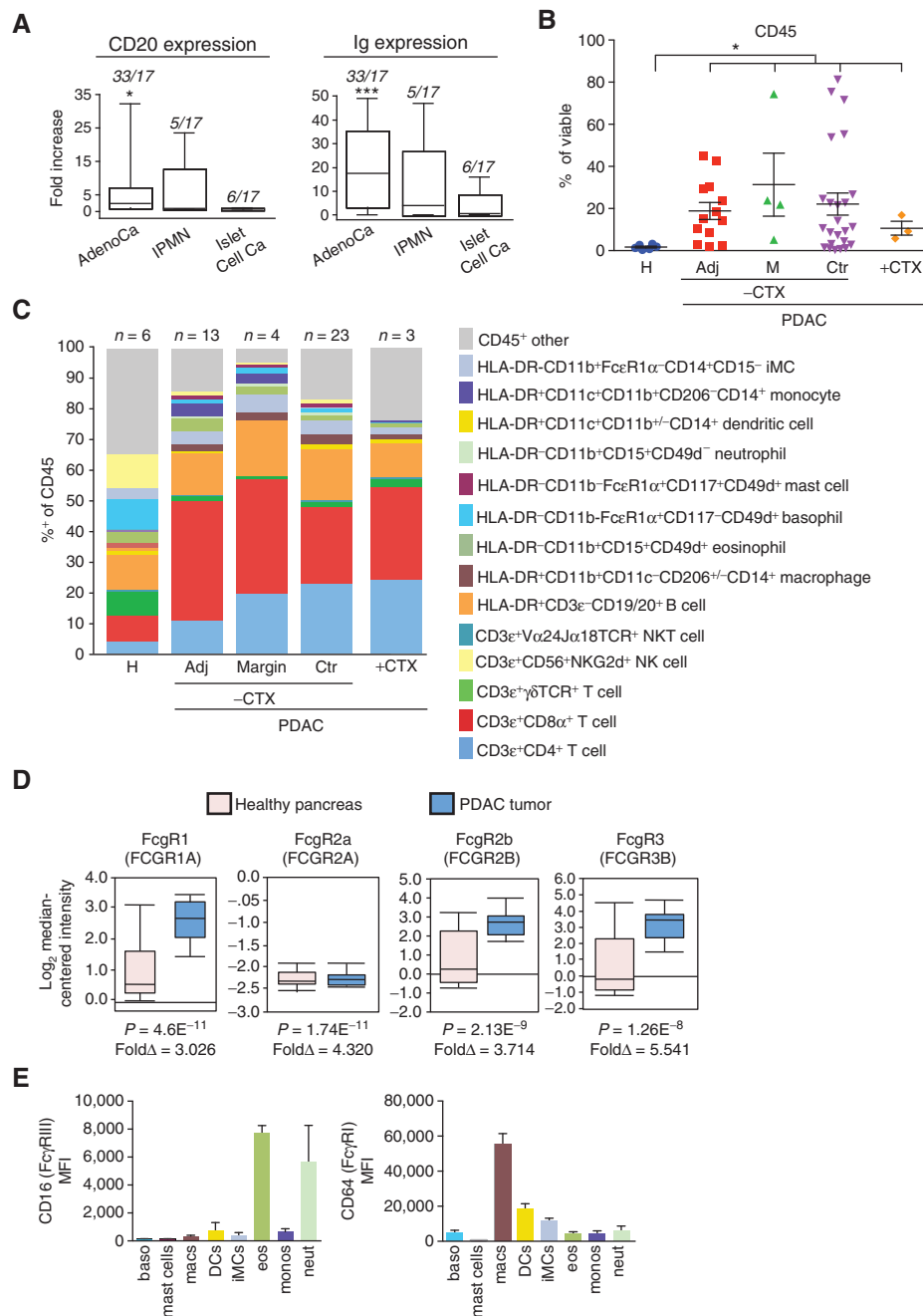


Figure 1. Leukocytes in human PDAC. **A**, relative CD20 and Ig mRNA expression in human pancreatic ductal adenocarcinoma (AdenoCa; $n = 33$), IPMN ($n = 5$), and islet cell carcinomas (Islet Cell Ca; $n = 6$), as compared with healthy pancreas tissue ($n = 17$) assessed by Affymatrix Human U133 Plus 2 microarrays. Data are represented as box-and-whisker plots depicting median fold-change value compared with normal tissue, displaying the first and third quartiles at the end of each box, with the maximum and minimum at the ends of the whiskers. Statistical significance was determined via the Wilcoxon rank-sum test with *, $P < 0.05$; ***, $P < 0.001$. **B**, FACS quantitation of CD45⁺ cells as a percentage of viable cells from pancreas tissues reflecting healthy (H) pancreata ($n = 6$), pancreas tissue adjacent to PDAC (Adj; $n = 13$), PDAC tumor margins (M; $n = 4$) and tumor centers (Ctr; $n = 23$) from patients who had not received prior chemotherapy (-CTX), and PDACs ($n = 3$) from patients treated with standard-of-care CTX (+CTX). Each data point reflects an individual piece of tissue. **C**, leukocyte complexity of healthy human pancreas ($n = 6$), and pancreas tissue isolated from patients with PDAC evaluated by polychromatic flow cytometry of single-cell suspensions and evaluated for expression of the lineage markers shown. Data represent mean leukocyte complexity for leukocyte lineages shown (right) in tumor tissue resected from healthy pancreata (H; $n = 6$), pancreata tissue adjacent to PDAC (Adj; $n = 13$), tissue resected from PDAC margins ($n = 4$) or tumor centers (Ctr; $n = 23$), and PDACs ($n = 3$) from patients treated with standard-of-care CTX (+CTX). Data reflecting individual populations is provided in Supplementary Fig. S1D. **D**, mRNA expression of FcγR isoforms from humans with healthy pancreas versus patients with PDAC tumors. Data were compiled from gene expression available in Oncomine (<https://www.oncomine.org>). P values and fold change in gene expression are shown. **E**, FACS histogram showing relative frequency of CD64 (FcγR1) and CD16 (FcγRIII) expression on leukocytes infiltrating human PDAC. Data shown are reflective of 20 human PDACs. Lineage markers for cell types shown are as indicated in C and reflect basophils (baso), mast cells, macrophages (macs), DCs, inflammatory monocytes (iMCs), eosinophils (eos), monocytes (monos), and neutrophils (neut). Adjacent (Adj) normal indicates tissue isolated from pancreas tissue proximal to resected PDAC tumors.

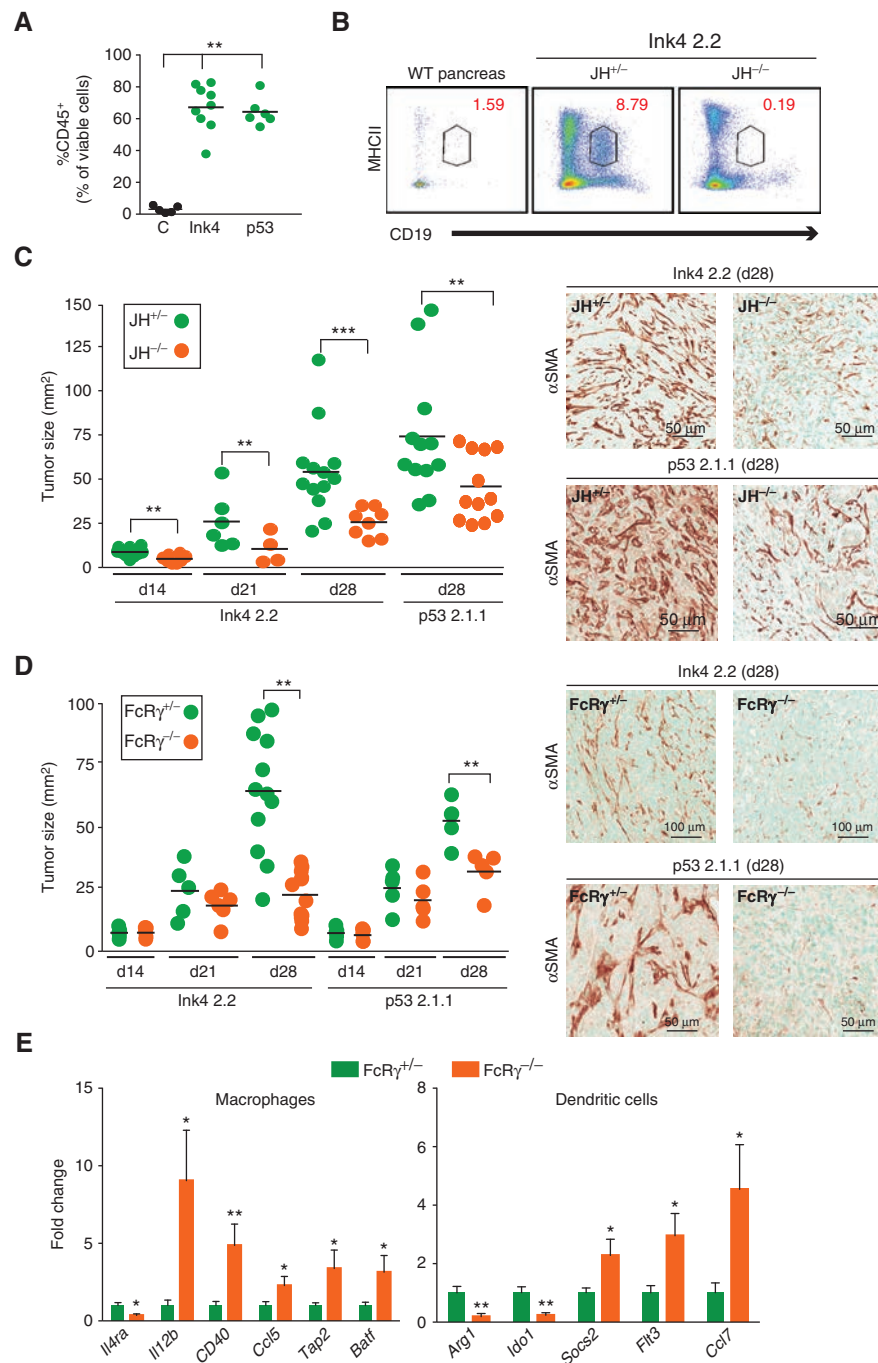


Figure 2. Orthotopic PDAC growth is regulated by B cells and Fc γ R-positive myeloid cells. **A**, murine PDAC cell lines, derived from *Pdx-Cre; LSL-Kras^{G12D}* mice harboring an *Ink4a/Arf^{fllox/+}* allele (Ink4 2.2) or a *p53^{fllox/+}* allele (p53 2.1.1), were injected orthotopically into the pancreas, and subsequent tumors evaluated by FACS for CD45-positive cellular infiltrates. Graph shows the percentage of CD45⁺ cells as a percentage of viable cells. **B**, representative CD19⁺MHCII⁺ FACS plot gated on viable CD45⁺ cells from tumor-naïve pancreas and Ink4 2.2-implanted PDAC tumors in syngeneic JH^{+/-} and JH^{-/-} mice evaluated 28 days after implantation. **C**, Ink4 2.2 and p53 2.1.1-derived PDACs were quantitatively evaluated in syngeneic JH^{+/-} and JH^{-/-} mice for tumor area in serial H&E-stained tissue sections reflecting tumors isolated on days 14, 21, and 28 after implantation. On right, representative photomicrographs reflecting immunodetection of α SMA in end-stage Ink4 2.2 and p53 2.1.1-derived orthotopic PDAC tumors. **D**, Ink4 2.2 and p53 2.1.1-derived PDACs were quantitatively evaluated in syngeneic Fc γ R^{+/-} and Fc γ R^{-/-} mice for tumor area in serial H&E-stained tissue sections reflecting tumors isolated on days 14, 21, and 28 after implantation. Right, representative photomicrographs reflecting immunodetection of α SMA in end-stage Ink4 2.2 and p53 2.1.1-derived orthotopic PDAC tumors. **E**, qRT-PCR analysis from cDNA reflecting FACS-purified macrophages (M0 = CD45⁺CD11b⁺MHCII⁺F4/80⁺Ly6C⁻) or DC (CD45⁺CD11b⁺MHCII⁺F4/80⁺CD11c⁺) from Ink4 2.2 PDAC-derived tumors harvested from day 21 Fc γ R^{+/-} ($n = 10$) or Fc γ R^{-/-} ($n = 8$) mice. Displayed are fold changes in genes that reached statistically significant differences. Data are compiled from two independent experiments. For graphs in **A**, **C**–**E**, statistical means are shown, with P values determined by either Student t test or one-way ANOVA when analyzing more than two groups, with *, $P < 0.05$; **, $P < 0.01$; ***, $P < 0.001$. For graphs in **C** and **D**, each data point reflects mean tumor size from one mouse based on quantitative morphometry of 5 FFPE sections, resulting from 3 independent experiments.

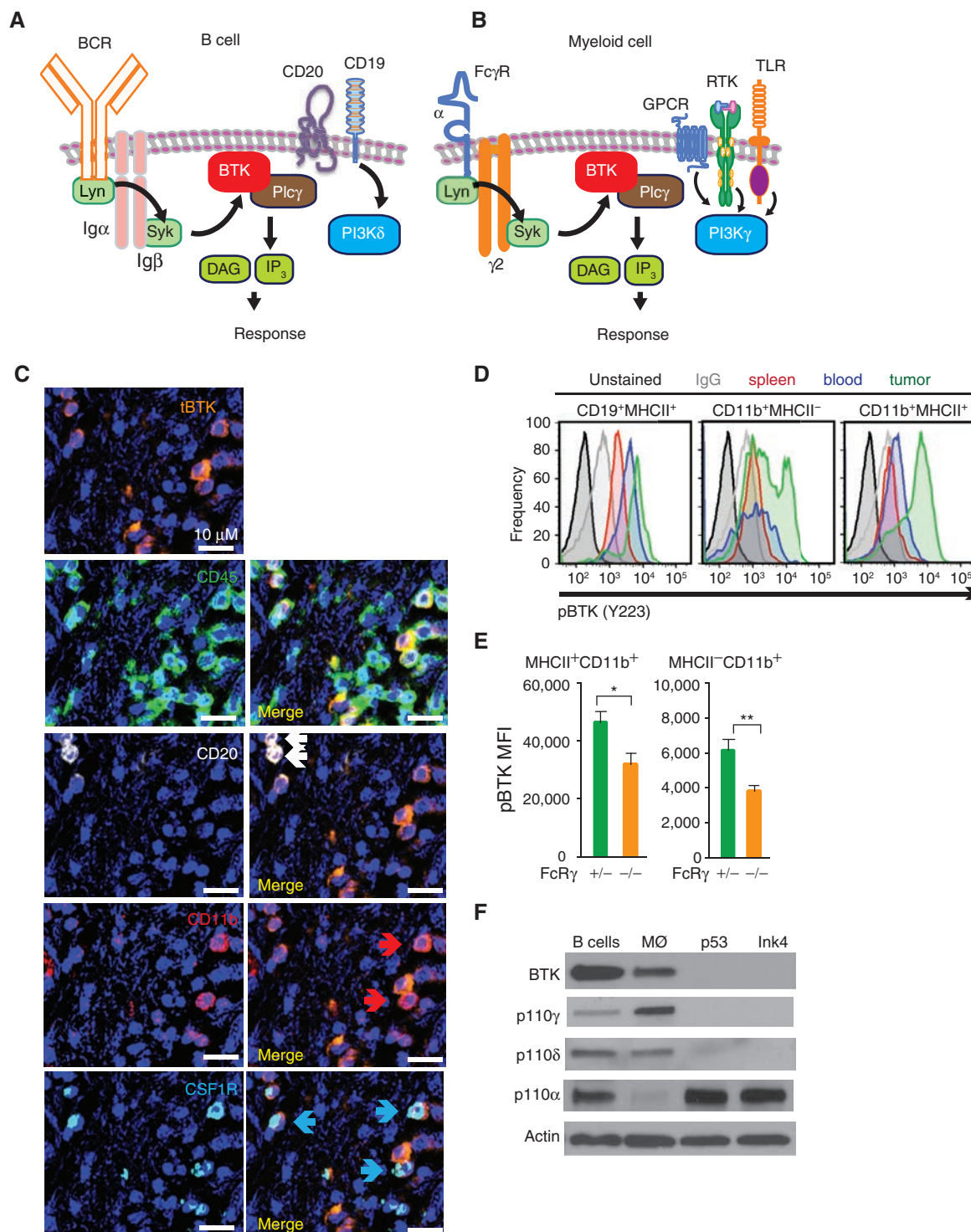


Figure 3. BTK and PI3K in PDAC-infiltrating B cells and myeloid cells. **A** and **B**, cartoons depicting BCR- and Fc γ R-activated BTK signaling in B cells and myeloid cells. **C**, representative photomicrograph showing immunodetection of BTK, CD45, CD20, CD11b, and CSF1R in a human PDAC FFPE section. Arrows in “merged” images indicate double-positive cells. Magnification is shown. **D**, intracellular FACS detection of activated phospho-BTK (pBTK; Y223) in single cells harvested from peripheral blood, spleen, and tumor tissue of Ink4 2.2-implanted syngeneic mice, gated on CD19⁺MHCII⁺ B cells, and CD11b⁺MHCII⁻ and CD11b⁺MHCII⁺ myeloid cells. Also shown are unstained and IgG1 isotype control stained cells. Representative data from one experiment ($n = 7$ mice) reflective of 2 independent experiments are shown. **E**, intracellular FACS detection of pBTK (Y223) in MHCII⁺CD11b⁺ and MHCII⁻CD11b⁺ cells isolated from end-stage Ink4 2.2 PDAC tumors from syngeneic Fc γ R^{+/-} or Fc γ R^{-/-} mice. Data from one representative experiment ($n = 8$ mice per experimental group) are shown and are reflective of 2 independent experiments. **F**, cropped Western blot images showing expression of BTK, PI3K γ (p110 γ), PI3K δ (p110 δ), PI3K α (p110 α), and actin in murine PDAC-derived B cells, primary murine macrophages (MØ), and cultured PDAC clones p53 2.1.1 (p53), and Ink4a 2.2 (Ink4).

leukocytes, CD20⁺ B cells, and CD11b⁺ and colony-stimulating factor 1 receptor (CSF1R)-positive myeloid cells (Fig. 3C; Supplementary Fig. S3A). In murine PDAC tumors, we identified activated BTK (pBTK) cells in single-cell suspensions, most prominently in tumor-resident CD19⁺MHCII⁺ B cells and CD11b⁺ myeloid cells (Fig. 3D). Relative to unstimulated cells, the mean fluorescent intensity (MFI) of pBTK significantly increased in B cells and myeloid cells following BCR and FcγRII/III stimulation, respectively (Supplementary Fig. S3B). Importantly, BTK activation was reduced in FcRγ-deficient myeloid cells infiltrating orthotopic PDAC tumors (Fig. 3E). As macrophage depletion via administration of a depleting colony-stimulating factor (CSF1) antibody (αCSF1 mAb; refs. 9, 20, 23; Supplementary Fig. S3C) and B-cell depletion through loss of the *JH* locus (Fig. 2C) significantly reduced PDAC tumor growth *in vivo*, we postulated that BTK⁺ B cells and macrophages were promoting PDAC growth.

PI3Kγ Activates Macrophage BTK to Promote PDAC Growth

As PI3Ks can activate BTK to promote phospholipase C (PLC)γ-dependent signaling in hematopoietic cells (21, 24), we explored the roles of BTK and PI3Ks in B cell-macrophage interactions during PDAC tumorigenesis. Four unique isoforms of class I PI3Ks (p110α, β, δ, and γ) regulate PI3K signaling in cells (2). We found that primary murine macrophages express high levels of BTK and PI3Kγ (p110γ), but lower levels of PI3Kδ (p110δ), whereas B cells express high levels of BTK, PI3Kα (p110α), and PI3Kδ, but low levels of PI3Kγ; neoplastic PDAC tumor cells express only PI3Kα and PI3Kβ (p110β; Fig. 3F; Supplementary Fig. S3D). As PI3Kγ and BTK are similarly expressed in myeloid cells, and the PI3K isoform p110γ selectively promotes PLCγ-dependent integrin α4β1 activation leading to myeloid cell recruitment to tumors (25), we speculated that PI3Kγ might activate BTK to promote myeloid cell recruitment during PDAC progression.

To characterize the interactions between PI3Kγ and BTK in myeloid cells, we first compared their roles in mediating integrin α4β1 activation and cell adhesion, processes that are required for myeloid cell trafficking into tumors (25, 26). To achieve this, we used pharmacologic inhibitors and siRNA-mediated knockdown of *Btk*, as well as pharmacologic and genetic disruption of p110γ (PI3Kγ). To inhibit BTK, we utilized an FDA-approved BTK inhibitor, PCI-32765 (ibrutinib; ref. 27). PCI-32765 has an IC₅₀ of 0.5 nmol/L for BTK and exhibits cross-reactivity to BLK and BMX (IC₅₀ = 0.5 nmol/L), ITK (IC₅₀ = 11 nmol/L), and TEC (IC₅₀ = 78 nmol/L; ref. 22). To inhibit p110γ, we utilized the investigational PI3Kγ/δ inhibitor TG100-115, which has an IC₅₀ of 83 nmol/L for PI3Kγ, 238 nmol/L for PI3Kδ, and >1,000 nmol/L for PI3Kα and PI3Kβ (25, 28).

We previously found that stromal cell-derived factor 1 (SDF1)α and IL1β induce adhesion of primary macrophages to vascular cell adhesion protein (VCAM)1-coated surfaces (21–23); both PCI-32765 and TG100-115 significantly suppressed SDF1- and IL1β-mediated cell adhesion, with IC₅₀ values of 10 nmol/L and 100 nmol/L, respectively (Fig. 4A and B). In support of these findings, *Btk* knockdown (Supplementary Fig. S4A), similar to *p110γ* deletion and knockdown (21–23), suppressed adhesion of primary myeloid cells to VCAM1

(Fig. 4C). PCI-32765 and p110γ inhibition also suppressed CD11b⁺ myeloid cell adhesion to vascular endothelial cell (EC) monolayers (Supplementary Fig. S4B), and PCI-32765 also suppressed B-cell adhesion to EC (Supplementary Fig. S4C). In addition, siRNA-mediated knockdown of PLCγ2, a key BTK and PI3Kγ signaling intermediate (21, 25; see schematic in Fig. 3A and B), suppressed myeloid cell adhesion (Supplementary Fig. S4D and S4E). Together, these findings support the hypothesis that PI3Kγ, BTK, and PLCγ2 regulate similar signaling pathways in myeloid cells that contribute to PDAC progression.

Based on these findings, we surmised that PI3Kγ might activate a BTK-signaling pathway to promote integrin α4β1 activation on macrophages prior to cell adhesion. In support of this, BTK inhibition, similar to PI3Kγ inhibition (25), suppressed integrin activation, as measured by cytokine-induced fluorescent VCAM1 binding to myeloid cells (Fig. 4D). In this assay, whereas VCAM1 binding to macrophages was rapidly stimulated by SDF1α or positive control Mn²⁺, VCAM1 binding was completely inhibited in the presence of PCI-32765 (Fig. 4D). Because BTK activation, as measured by autophosphorylation on Y223, was suppressed in macrophages lacking PI3Kγ (p110γ^{-/-}; Supplementary Fig. S4F), we concluded that PI3Kγ activates a BTK-PLCγ2 pathway to promote integrin activation, myeloid cell adhesion and, potentially, myeloid cell recruitment to tumors *in vivo*.

Because we previously reported that PI3Kγ regulates protumorigenic properties of macrophages *in vivo* (25), we asked whether PI3Kγ activated BTK to promote protumor macrophage polarization. IFNγ/lipopolysaccharide (LPS) signaling induces macrophage expression of T_H1 cytokines, including IL12, TNFα, IL6, IL1β, and nitric oxide synthase (NOS)2, and inhibits expression of T_H2 immune-suppressive cytokines, including Arginase (ARG)1 and TGFβ *in vitro*, whereas IL4 signaling instead inhibits expression of T_H1 cytokines and stimulates expression of T_H2 factors *in vitro* (29, 30). We undertook an analysis of relative mRNA levels in IFNγ- or IL4-stimulated control and p110γ^{-/-} or PCI-32765-treated macrophages by RT-PCR. Analysis of the change in mRNA levels between control and p110γ^{-/-} or PCI-32765-treated macrophages indicated that genetic or pharmacologic inhibition of either PI3Kγ or BTK induced T_H1 skewing of IFNγ/LPS-stimulated macrophages, as expression of *Il12*, *Il6*, *Tnfa*, *Il1b*, and *Nos2* was enhanced, and expression of *Arg1*, *Il10*, and *Ccl2* was reduced (Fig. 4E; Supplementary Fig. S4G and S4H). Inhibition of either PI3Kγ or BTK by pharmacologic or genetic approaches similarly induced T_H1 skewing of IL4-stimulated macrophages while also inhibiting *Il1b* and *Tnfa* expression (Fig. 4F; Supplementary Fig. S4I). The combination of BTK inhibitors with PI3Kγ^{-/-} macrophages had little additional effect on T_H1 skewing of macrophage gene expression profiles (Fig. 4F), indicating that BTK and PI3Kγ regulate similar macrophage polarization pathways. Importantly, these observations also reveal that PI3Kγ and BTK similarly promote T_H2 macrophage polarization and restrain T_H1 polarization, indicating that these kinases may promote protumor T_H2 macrophage polarization *in vivo*.

Because macrophage FcγR signaling promotes PDAC growth (Fig. 2), we investigated the consequences of FcγR cross-linking on macrophage polarization by incubating

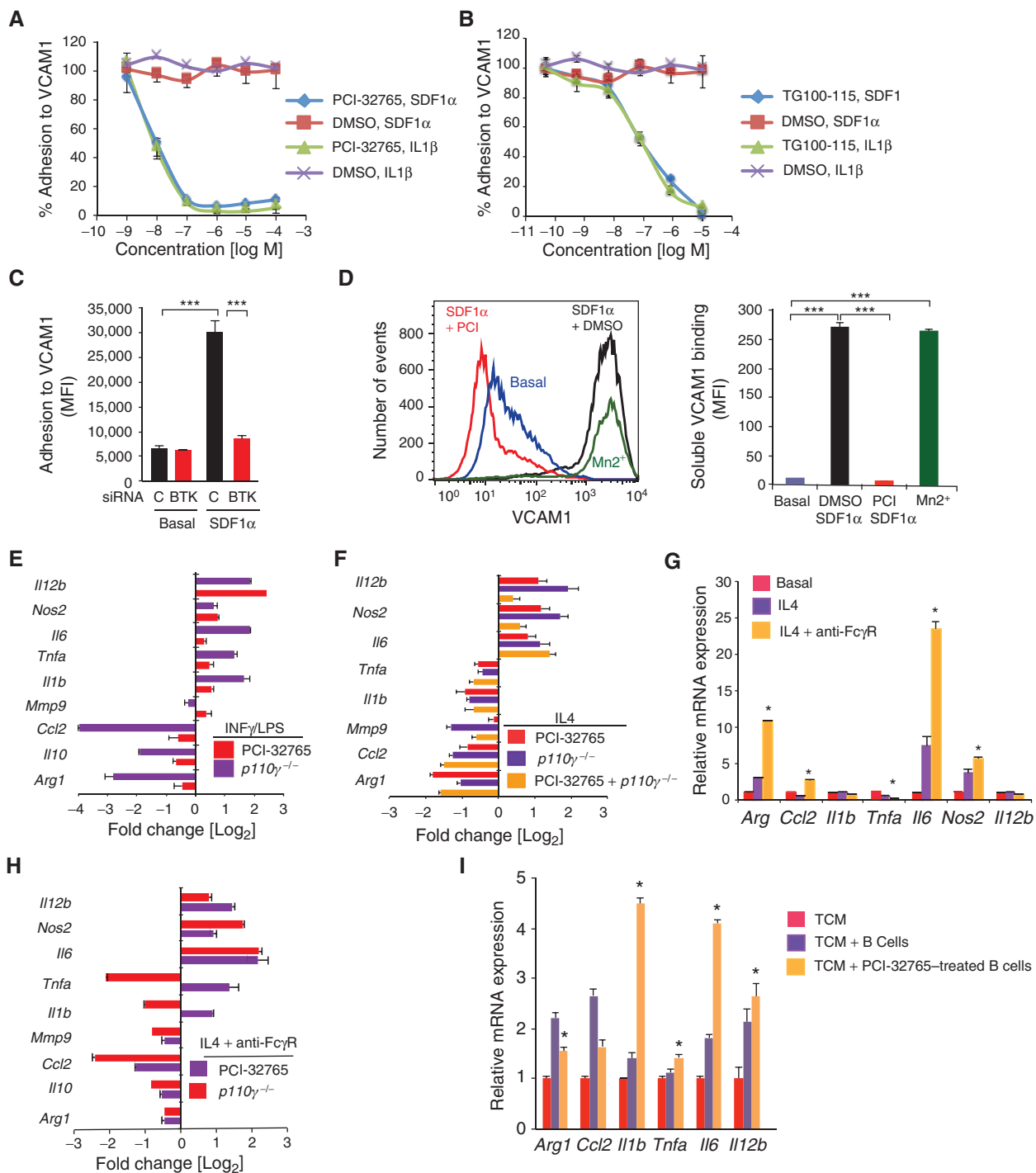


Figure 4. FcR γ signaling regulates BTK activation and mediates PDAC growth. **A** and **B**, effect of the BTK inhibitor PCI-32765 (**A**) and the p110 γ inhibitor TG100-115 (**B**) versus vehicle control (DMSO) on IL1 β - and SDF1 α -stimulated adhesion of primary myeloid cells to VCAM1 ($n = 3$). **C**, effect of siRNA-mediated BTK knockdown on SDF1 α -stimulated myeloid cell adhesion to VCAM1 ($n = 3$). **D**, effect of PCI-32765 (PCI) on SDF1 α -induced integrin $\alpha 4\beta 1$ activation, as detected by binding of fluorescent VCAM1 to myeloid cells ($n = 3$); left, FACS profiles and right, quantification of mean fluorescence intensity. Positive control, extracellular Mn $^{2+}$ treatment. **E** and **F**, Log $_2$ fold change of gene expression in (**E**) LPS/IFN γ *in vitro*-polarized macrophages treated with PCI-32765 or p110 $\gamma^{-/-}$ macrophages, (**F**) p110 $\gamma^{-/-}$, PCI-32765-treated, and p110 $\gamma^{-/-}$ PCI-32765-treated IL4 *in vitro*-polarized primary murine macrophages ($n = 3$). **G**, relative mRNA expression of macrophages polarized with IL4 or IL4+FcR γ cross-linking ($n = 3$). **H**, Log $_2$ fold change of gene expression in IL4-stimulated FcR γ -cross-linked p110 $\gamma^{-/-}$ or PCI-32765-treated primary murine macrophages ($n = 3$). **I**, relative mRNA expression of macrophages cocultured in p53 2.1.1 tumor cell-conditioned medium (TCM) with tumor-derived B cells ($n = 3$) or PCI-32765-treated B cells. Data shown are mean \pm SEM of biological replicates and were validated in 3 or more separate experiments. Significance testing was performed by one-way ANOVA with Tukey *post hoc* testing for multiple pairwise testing or by the Student *t* test, where $P > 0.05$ unless otherwise specified; *, $P < 0.05$; **, $P < 0.01$; ***, $P < 0.001$. For mRNA expression studies, $P < 0.01$ unless otherwise indicated.

macrophages with anti-Fc γ R antibodies followed by secondary antibodies. Fc γ R cross-linking of IL4-polarized macrophages enhanced T_{H2} skewing, as macrophages displayed enhanced expression of key T_{H2} factors, including *Arg1* and *Ccl2* (Fig. 4G). Importantly, inhibition of either PI3K γ or BTK suppressed Fc γ R-stimulated T_{H2} cytokine expression and promoted T_{H1} cytokine expression, with the exception that PI3K γ inhibition suppressed, while BTK inhibition stimulated, *Tnfa* and *Il1b* expression (Fig. 4H). These minor differences in Fc γ R-stimulated gene expression indicate that PI3K γ regulates both BTK-dependent and BTK-independent gene expression pathways. Taken together, these results support the hypothesis that PI3K γ activates BTK to promote macrophage T_{H2} polarization.

We previously reported that B cell-derived Ig containing immune complexes stimulate Fc γ R cross-linking to promote macrophage T_{H2} cytokine expression (19). To determine if BTK regulated B cell-directed expression of T_{H2} cytokines in macrophages, we cocultured PDAC-derived B cells with primary macrophages in coculture chambers *in vitro*. Under these conditions, B cells and macrophages were separated by a filter allowing the passage of only macromolecules between chambers. In the presence of PDAC cell-conditioned medium, tumor-derived B cells enhanced macrophage T_{H2} skewing; however, pretreatment of PDAC-derived B cells with PCI-32765 suppressed this and instead enhanced expression of T_{H1} cytokines (Fig. 4I). As B cell-derived immune complexes promote macrophage T_{H2} cytokine expression (8), these results indicate that B cells promote the immunosuppressive, protumor properties of macrophages in a manner that depends on BTK in both B cells and macrophages.

To evaluate the relative contributions of BTK in B cells and macrophages during tumor progression *in vivo*, B cells isolated from spleens of PDAC (p53 2.1.1)-bearing animals or Gr1⁺CD11b⁺ myeloid cells (Supplementary Fig. S5A) isolated from tumors of PDAC (p53 2.1.1)-bearing animals were incubated with PCI-32765 or vehicle, mixed with tumor cells, and implanted in animals. Untreated B cells and myeloid cells had no significant effect on tumor growth, whereas pretreatment of B cells or myeloid cells with BTK inhibitor prior to implantation significantly suppressed tumor growth (Fig. 5A). These results support the hypothesis that BTK in both B cells and myeloid cells promotes PDAC tumor growth.

As neither BTK nor PI3K γ inhibitors directly affected the viability of macrophages (Supplementary Fig. S5B) or PDAC tumor cells (Supplementary Fig. S5C and S5D), we evaluated whether PI3K γ regulated BTK activity during PDAC growth *in vivo* by systemically treating WT and p110 γ ^{-/-} mice bearing p53 2.1.1 PDAC tumors with or without PCI-32765 (Fig. 5B). Analogous to clinical scenarios observed in patients (31), mice receiving PCI-32765 exhibited transient lymphocytosis in the peripheral blood of tumor-bearing mice that resolved by the study termination (Supplementary Fig. S5E). PDAC tumor growth was similarly suppressed in p110 γ ^{-/-} animals and in WT mice treated with PCI-32765, whereas PCI-32765 treatment of p110 γ ^{-/-} mice had no additive effect on tumor growth (Fig. 5C). Importantly, p110 γ deletion and PCI-32765 inhibitor treatment suppressed B-cell and CD11b⁺ myeloid cell infiltration (Fig. 5D and E; Supplementary Fig. S5F) as predicted by results from the *in vitro* cell adhesion studies

(Fig. 4A and B). p110 γ deletion and PCI-32765 treatment also increased CD8⁺ T-cell presence in tumors (Fig. 5F).

To evaluate the effect of combined treatment of PDAC tumors with PI3K γ and BTK pharmacologic inhibitors, we treated mice bearing orthotopic p53 2.1.1 PDAC tumors with PI3K γ and BTK inhibitors alone, together, or each in combination with gemcitabine (Gem; Fig. 5G). TG100-115 and PCI-32765 both suppressed PDAC tumor growth, as reflected in weights of pancreata 28 days after inoculation, but the combination of the two inhibitors had no additive effect (Fig. 5G). Gem monotherapy suppressed tumor growth as measured by pancreas weight, whereas Gem plus TG100-115 or Gem plus PCI-32765 had no additional impact on overall pancreas weight (Fig. 5G). However, histologic examination of end-stage tumors revealed little residual live tumor in pancreata treated with Gem plus PCI-32765 or TG100-115, indicating additive effects of the two therapies with Gem (Fig. 5H and I). Importantly, PI3K γ and BTK inhibitors suppressed CD11b⁺ myeloid cell infiltration (Fig. 5J; Supplementary Fig. S5G) and increased CD8⁺ T-cell residency of tumors (Fig. 5J), similar to results observed in Fig. 5E and F. The combination of PI3K γ and BTK inhibitors had no additional effects beyond those of each inhibitor alone, supporting the conclusion that PI3K γ and BTK regulate the same pathway *in vivo* as well as *in vitro* (Fig. 4E-H). In addition, all Gem-treated pancreata exhibited fewer CD11b⁺ and CD8⁺ T cells than other treatments, as very little tumor tissue remained in these pancreata after 28 days (Fig. 5I-K). As PI3K γ and BTK inhibition suppressed T_{H2} and stimulated T_{H1} cytokine expression in *in vitro* cultured macrophages (Fig. 4E-I), in the tumor microenvironment (Fig. 5L), and in tumor-derived myeloid cells (Supplementary Fig. S5H), these studies indicate that BTK and PI3K γ regulate macrophage and T-cell programming *in vivo* as well as *in vitro*. Together these data support the conclusion that PI3K γ and BTK promote a pathway leading to T_{H2} polarization during PDAC progression. Furthermore, these data indicate that PI3K γ and BTK inhibitors could be useful therapeutic approaches to treat early PDAC tumors.

Clinically, patients with PDAC typically present at late stage; thus, we sought to determine if therapeutic administration of PCI-32765 was efficacious in late-stage PDAC tumors as monotherapy, or in combination with Gem (Fig. 6A). PDAC growth in mice treated with combination PCI-32765/Gem administered at a late stage resulted in significantly reduced tumor size at end stage (Fig. 6B). Decreased tumor burden was associated with reduced presence of CD45⁺ leukocytes (Fig. 6C; Supplementary Fig. S6A), associated with dynamic changes in the B-cell compartment whereby Gem treatment reduced the presence of memory B cells, BTK inhibitor (BTKi) resulted in increased frequency of T2 and B1b cells and reduced frequency of follicular and marginal zone B cells (Supplementary Fig. S2D), and decreased desmoplasia (Fig. 6D; Supplementary Fig. S6A). Importantly, we also observed a significant increase in the intratumoral frequency of granzyme B^{hi}, IFN γ ⁺, and extracellular CD107a⁺ CD8⁺ T cells, indicative of their recent activation and degranulation (Fig. 6E-G; Supplementary Fig. S6A). In agreement with these data, there was an enhanced presence of programmed death (PD)-1⁺EOMES⁺ late effector and PD-1⁻EOMES⁻ short-term memory CD8⁺ T-cell phenotypes (Fig. 6H; Supplementary Fig. S6B), that

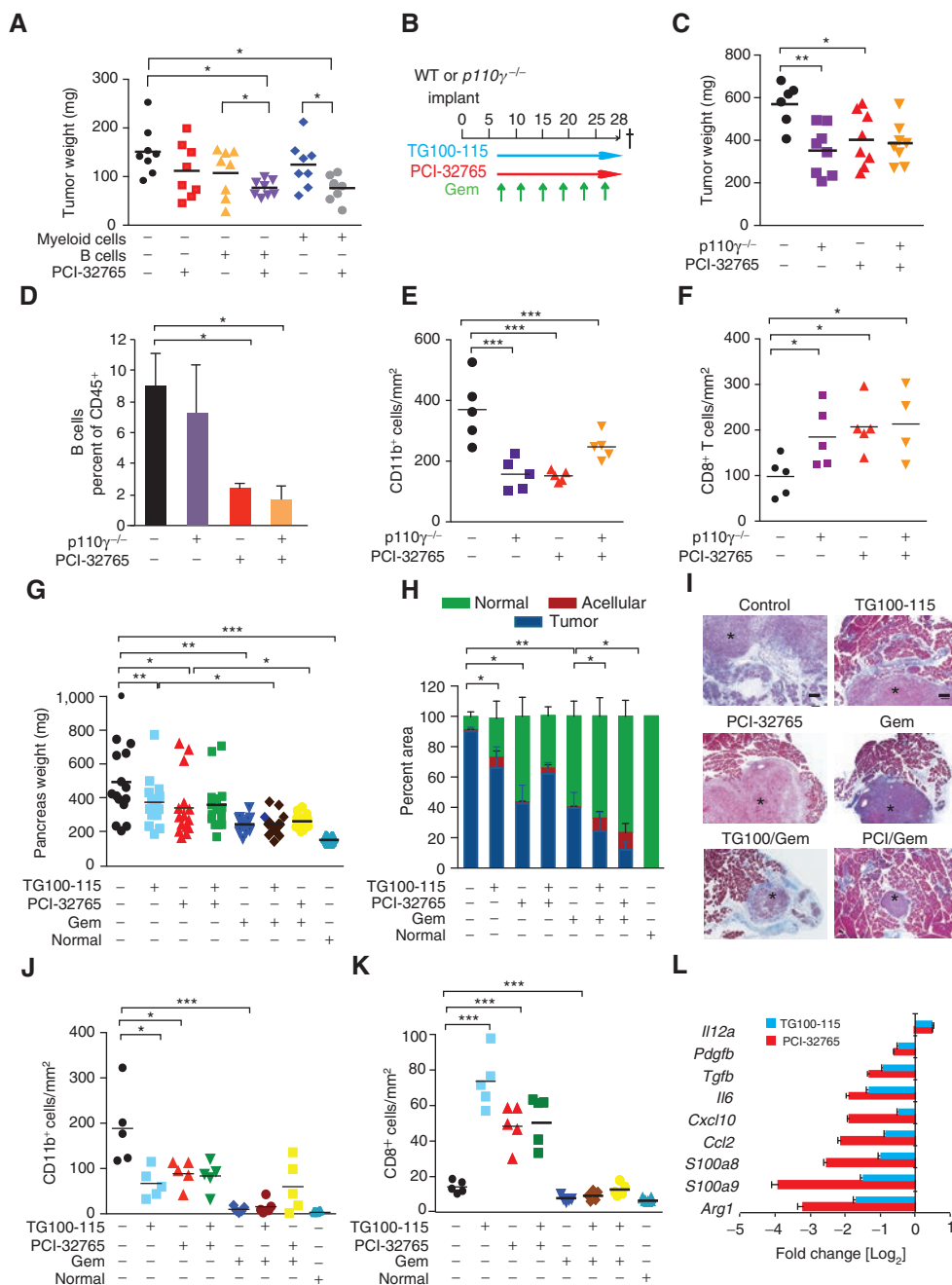


Figure 5. PI3K γ and BTK promote PDAC progression. **A**, tumor burden in mice implanted with admixed p53 2.1.1 cells together with PCI-32765- or vehicle-pretreated B cells or myeloid cells as compared with untreated or PCI-32765 after implantation treatment alone. **B**, schemas for early treatment schedule for PDAC-bearing mice with administration of PCI-32765 in drinking water (0.016% w/v) and/or the p110 γ inhibitor TG100-115 (2.5 mg/kg b.i.d. given i.p.) beginning on day 7 after implantation, and gemcitabine (Gem; 15 mg/kg, i.v.) in p53 2.1.1-derived PDAC-bearing mice. Cross signifies end point or death. **C**, end-stage p53 2.1.1 PDAC tumor weights from syngeneic PI3K γ -deficient (*p110 γ ^{-/-}*) or WT mice treated with or without PCI-32765 ($n = 10$ –15/mice per experimental group). **D**, tumor-derived B cells as a percentage of CD45⁺ cells in treated tumors from **C**, as determined by FACS analysis. **E**, number of CD11b⁺ cells/mm² in treated tumors from **C**. **F**, number of CD8⁺ T cells/mm² in treated tumors from **C**. **G**, effect of TG100-115, PCI-32765, gemcitabine (Gem), and combinations of these agents on growth to end stage of orthotopic p53 2.1.1 PDAC tumors ($n = 10$ –15/mice per experimental group) depicted as total pancreas weight after 3 weeks of treatment as compared with pancreas weight of tumor-naïve mice. **H**, percent residual tumor, normal acinar tissue, and acellular fibrotic tissue in pancreata of tumors depicted in **G**. **I**, representative photomicrographs showing Masson's trichrome stained images of PDAC tumors (*) treated as shown reflecting quantitation in **G** and **H**. Scale bars, 200 μ m. **J**, number of CD11b⁺ cells/mm² in treated tumors depicted in **C**, compared with normal pancreata. **K**, CD8⁺ T cells/mm² in treated tumors depicted in **C**. **L**, log base 2 fold change in gene expression in tumors between control and TG100-115 or control and PCI-32765 treatments ($n = 15$). mRNAs for which TG100-115-treated tumors showed statistically significant differences from control tumors are shown. Data shown are mean \pm SEM of biologic replicates and were validated in 3 or more separate experiments. Significance testing was performed by one-way ANOVA with Tukey *post hoc* testing for multiple pairwise testing or by Student *t* test, where $P > 0.05$ unless otherwise specified, *, $P < 0.05$; **, $P < 0.01$; ***, $P < 0.001$. ns, not statistically different. For **A**, **C**, **E**–**G**, **J** and **K**, each data point reflects an individual tumor with statistical means shown. For mRNA expression studies, $P < 0.01$ unless otherwise indicated.

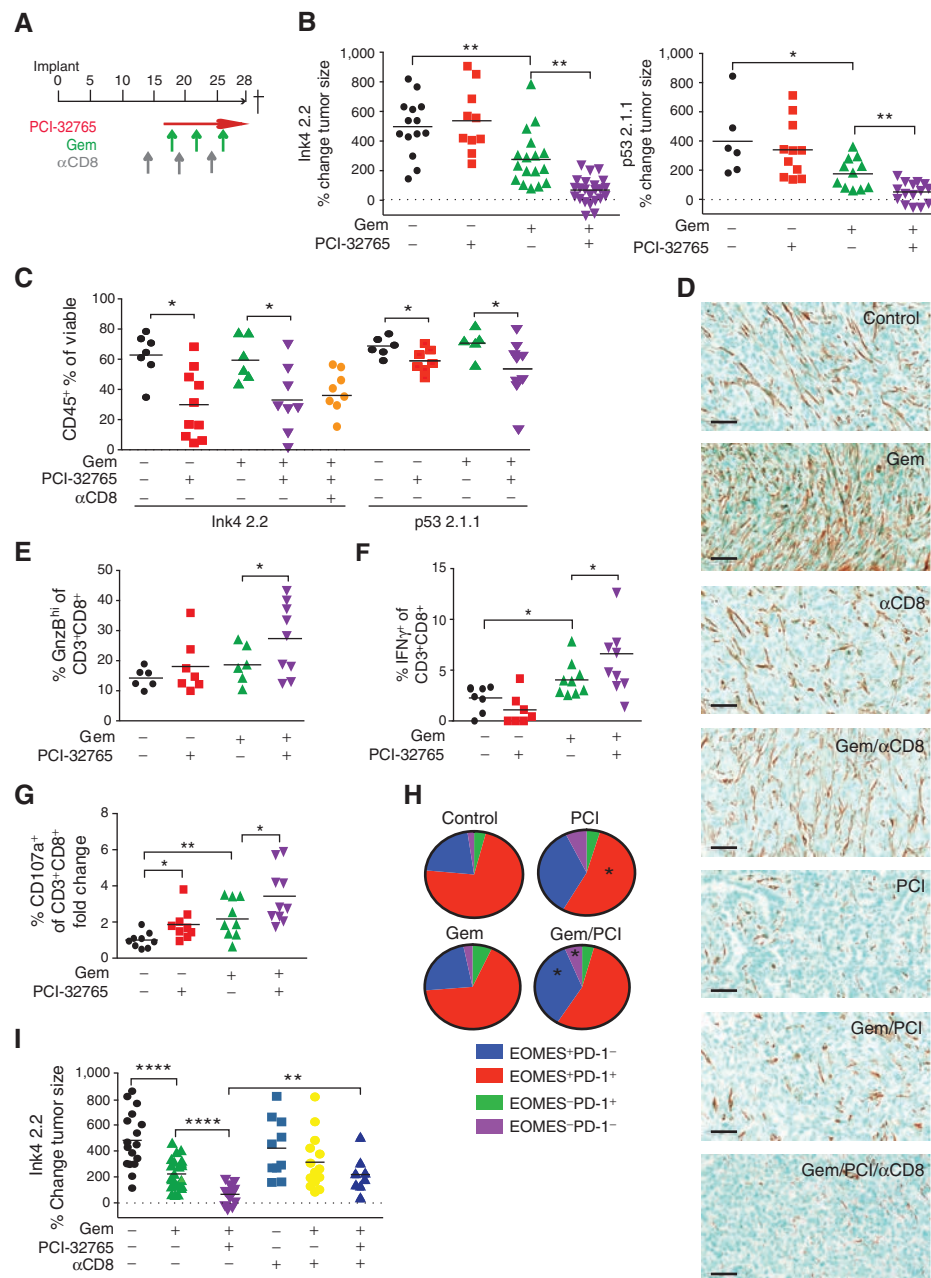


Figure 6. BTK-activated signaling regulates PDAC tumorigenesis. **A**, schemas for therapeutic administration of PCI-32765 (in drinking water [0.16% w/v]) beginning on day 14 after implantation and gemcitabine (Gem; 15 mg/kg, i.v., beginning on day 18) to late-stage PDAC tumor-bearing mice. 500 μ g depleting α CD8 mAb antibody administered i.p. on days 15, 20, and 25. Cross signifies end point or death. **B**, percentage change in Ink4 2.2 (left) or p53 2.1.1 (right) tumor size from days 14 to 27 after implantation measured by ultrasonography and assessed following treatment with vehicle (-), PCI-32765, or Gem, and combinations as indicated. For Ink4 2.2, data from 3 independent experiments are shown, reflective of 5 independent experiments. For p53 2.1.1, data from one experiment are shown and are representative of 2 independent experiments. **C**, CD45⁺ leukocyte frequency from end-stage tumors as a percentage of total viable cells determined by FACS analysis of single-cell suspensions of tumors from treatment groups indicated. Data from 2 independent experiments are shown and are representative of 5 independent studies. **D**, representative photomicrographs showing immunodetection of α SMA in mice bearing end-stage Ink4 2.2 PDAC tumors treated as shown. Scale bars, 100 μ m. **E**, percentage of granzyme B-positive (GnzB) cells of CD3⁺CD8⁺ cells as determined by FACS of end-stage Ink4 2.2 PDAC tumors treated as shown. Data from 2 independent experiments are shown and are representative of 4 independent studies. **F**, percentage of IFN γ ⁺CD8⁺ T cells of CD3⁺CD8⁺ cells as determined by intracellular FACS assessment of ex vivo-stimulated Ink4 2.2 PDAC tumors harvested from mice at day 23 after implant. Data from 2 independent experiments are shown. **G**, fold change of percent of CD107a⁺CD8⁺ T cells of CD3⁺CD8⁺ cells analyzed by FACS of Ink4 2.2 PDAC tumors harvested from mice at day 23 after implant. Data from 2 independent experiments are shown. **H**, FACS analysis of Ink4 2.2 tumors from day 23 time points for percentages of PD-1⁺EOMES⁺ populations of CD3⁺CD8⁺ T cells. Data from 2 independent experiments are shown. Statistical significance was determined using the Student *t* test or one-way ANOVA when analyzing more than two groups. **I**, percentage change in Ink4 2.2 tumor size from days 14 to 27 after implantation measured by ultrasonography and assessed following treatment with vehicle (-), PCI-32765, or Gem, and combinations in mice also administered depleting monoclonal antibodies for CD8⁺ (α CD8) T cells as indicated. Data from 2 independent experiments are shown. *, *P* < 0.05; **, *P* < 0.01; ***, *P* < 0.001. For **B-C** and **E-G** and **I**, each data point reflects an individual tumor, with statistical means shown.

correlated with T_H1 -skewing of BTKi-treated tumors (Fig. 5L). This increased presence of effector $CD8^+$ T-cell phenotypes was functionally significant as $CD8^+$ T-cell depletion reinstated tumor growth to levels similar to Gem-treated mice (Fig. 6I; Supplementary Fig. S6C), without reinstating the $CD45^+$ leukocyte infiltration (Fig. 6C) or desmoplasia (Fig. 6D) observed in untreated tumors. Taken together, these results indicate that myeloid cell $PI3K\gamma$ activates BTK, thereby promoting myeloid cell recruitment to PDACs and T cell-mediated immune suppression, and, importantly, indicate that pharmacologic inhibition of $PI3K\gamma$ or BTK activates a T_H1 immune response that suppresses tumor growth.

DISCUSSION

Pancreatic ductal adenocarcinoma is traditionally thought to be an immunologically silent malignancy, but recent therapeutic strategies have demonstrated that effective immune-mediated tumor cell death can be invoked to combat disease dissemination (32–34). The fundamental principle of these strategies is that $CD8^+$ T cells can be mobilized to recognize and eliminate malignant cells if suppressive barriers to immunity are abated. Data presented herein reveal a critical role for B cells and $Fc\gamma$ -activated myeloid cells, and in particular macrophages, in regulating functionality of $CD8^+$ T cells in PDAC, and identify BTK and $PI3K\gamma$ as key regulators of tumor immune suppression. Our studies demonstrate that both human and murine PDACs exhibit increased BTK activation in tumor-resident $CD20^+$, $CD11b^+$ and $Fc\gamma RI/III^+$ cells relative to leukocytes in the periphery. BTK or $PI3K\gamma$ inhibition as monotherapy in early-stage PDAC, or in combination with Gem in late-stage PDAC, slowed progression of orthotopic tumors in a manner dependent on T cells. Coincident with slowed tumor growth, the percentage of $CD8^+$ T cells with enhanced effector molecule expression increased in PDAC tumors that were functionally significant, as $CD8^+$ T-cell depletion eliminated benefits of combined BTK inhibitor/Gem therapy. An increase in effector and memory $CD8^+$ T-cell phenotypes was also observed midway through therapy, and thus consistent with other reports regarding $CD8^+$ T-cell responses to various immunotherapies (35). Based on these data and reports from other groups (36, 37), we anticipate that targeted inhibition of BTK with therapies like ibrutinib may synergize with immune checkpoint inhibitors and/or select anticancer vaccines to further bolster T-cell activation for long-term durable antitumor immunity (36). Notably, this hypothesis is currently being tested in patients with PDAC and squamous cell carcinoma of the head and neck in two clinical trials (ClinicalTrials.gov Identifiers: NCT02436668 and NCT02454179).

Although protumorigenic activities of B cells have not been widely investigated, we and other groups have reported direct and indirect protumorigenic roles for tumor-infiltrating as well as peripheral B cells. In squamous carcinomas and melanomas, humoral immunity and IL10-secreting B1 cells induce T_H2 -type programming of diverse myeloid cell types that foster tumor angiogenesis and $CD8^+$ T-cell suppression (9, 19, 38, 39). In B cell-infiltrated prostate cancers (40), immunosuppressive B cells and plasmocytes promote survival of androgen-independent prostatic epithelial cells via

lymphotoxin-mediated $NF\kappa B$ regulation (41), and inhibit the efficacy of immunogenic CTX by IL10 and immune checkpoint-mediated suppression of CTLs (42). CTL suppression in these contexts is consistent with *in vitro* data revealing that $IFN\gamma$ release from $CD8^+$ T cells and NK cells is increased when B cells are absent, whereas presence of B cells or B cell-derived IL10 is associated instead with reduced $IFN\gamma$ (43). Results reported herein lend further support for the role B cells play in mediating tumorigenesis and response to cytotoxic therapy and further identify BTK as a tractable target for anticancer therapy. Based on decreased presence of $IgM^{lo}CD23^+CD5^-$ follicular and $IgM^{lo}CD23^-$ memory B cells correlating with improved outcome and increased CTL bioactivity in BTKi-treated PDAC-bearing mice (Supplementary Fig. S2E), we anticipate operative activities for these B-cell subsets either in directly driving PDAC-associated T-cell suppression or in regulating CTL-mediated responses to cytotoxic therapy. At earlier stages of PDAC progression, however, IL35-producing B cells promote RAS-driven neoplasia (44) and B1b cell recruitment that are regulated by oxygen-sensing programs, that together slow early PDAC progression (45), and consistent with our results revealing dampened PDAC growth in B cell-deficient mice (Fig. 2). Together, these studies support both direct and indirect effects of B cells in regulating discrete aspects of tumorigenesis culminating in regulation of T-cell responses to neoplasia and cytotoxic therapy.

While identifying BTK as a B cell-intrinsic target, studies herein further identify macrophage BTK, and its regulation by $Fc\gamma$ - and $PI3K\gamma$ -mediated signaling, with subsequent effects on macrophage polarization, immune suppression, and induction of desmoplastic stroma. Although one prior study linked the class IA $PI3Ks$ to BTK activation in B cells, recent studies have reported that these proteins regulate similar but distinct signaling pathways in B cells (33, 34). Our studies instead reveal the selective role of the class IB $PI3K$ isoform $PI3K\gamma$ in regulating BTK to control the macrophage response to the tumor microenvironment. PDACs from BTKi and $PI3K\gamma$ inhibitor-treated mice exhibited a T_H1 -polarized phenotype with mRNAs encoding stimulators of $CD8^+$ T-cell cytotoxic activity. These observations are similar to antipathogen immunologic states and are necessary for immunogenic cell death of tumor cells (46), further supporting the hypothesis that BTK signaling regulates macrophage functionality and ultimately immunosuppression in PDAC tumors. Enhanced antitumor responses were observed when tumor-bearing mice were treated with BTKi therapy for an extended period of time commencing when PDAC tumors were small, as compared with later/larger stage tumors, supporting the general tenet that earlier detection and therapy in PDAC improves outcome.

Regarding BTK-regulated desmoplastic responses in PDACs, data presented herein are consistent with reported roles for macrophages in regulating muscle fibrosis and pancreatitis-associated fibrosis via pathways involving Arginine, $TGF\beta$, MMP9, IL10, and other T_H2 -type proteins (47, 48). Masso-Valles and colleagues also recently reported an important role for mast cells expressing BTK in regulating desmoplastic stroma of PDAC tumors (37). Although murine PDAC tumors evaluated herein did exhibit significant presence of mast cells, BTK inhibition did not alter the presence

of degranulating mast cells within tumor stroma (Supplementary Fig. S6D). Thus, if BTK regulates mast cell-induced desmoplasia, it likely does so via regulation of a protein secretion pathway, as opposed to a degranulation-mediated mechanism. Moreover, because CD8⁺ T-cell depletion of PCI-32765/Gem-treated mice reversed the benefit of combination therapy (Fig. 6I), without affecting decreased desmoplasia of treated tumors (Fig. 6D), these data indicate that decreased PDAC tumor growth due to BTK inhibition is dependent on B-cell and/or myeloid cell reprogramming and bolstering of T_H1-type immune responses, and independent of the desmoplasia that is characteristic of PDAC tumors.

Macrophage activation and polarization state are subject to a multitude of signals distinct in various tumor microenvironments. In mammary carcinomas, macrophages are recruited to tumor parenchyma by CSF1 expressed by mammary epithelial cells (49) and then polarized to a T_H2 effector state following stimulation by IL4 produced by infiltrating CD4⁺ T cells (50, 51). T_H2-skewed macrophages in turn indirectly regulate CD8⁺ T-cell functionality via their high-level expression of IL10, thereby impairing DC maturation and expression of IL12 (20). In contrast, macrophages in SCCs acquire a protumoral T_H2-type phenotype following Ig-containing immune complex activation of FcγR receptors (19), which in turn represses expression of macrophage-derived chemokines required for CD8⁺ T-cell infiltration (9). Whereas some of this same biology is preserved between pancreas and cutaneous microenvironments, other facets may play a more significant role in the pancreas, including mechanisms regulating B1b-cell recruitment into areas of hypoxia (45), and/or downstream of oncogenic RAS and CXCL13 (44). Future studies will determine why these tissue-specific differences exist, the appropriate patient populations likely to respond to these immunotherapy strategies, molecular mechanisms underlying paracrine BTK regulation of CD8⁺ T-cell functionality, and the degree to which mast cells and macrophages differentially play a role downstream of BTK in regulating desmoplasia associated with PDAC tumorigenesis. As the BTK inhibitor ibrutinib is FDA approved for the treatment of leukemia (27), our studies indicate that BTK inhibitors could be rapidly evaluated as new therapeutic agents for pancreatic cancer.

METHODS

Freshly Isolated Human PDAC Samples and Peripheral Blood

All human samples for IHC, pathology, FACS, and plasma analysis were obtained and studied under informed consent in accordance with the Declaration of Helsinki and acquired through the Oregon Pancreatic Tumor Registry and IRB protocol #3609.

Human PDA Tissue Microarray

Microarray data reflecting *CD20* and *Ig* mRNA in human tumor samples were queried from a commercially available data set (Bio-Express System, Gene Logic) originally generated on the Human Genome U133 Plus 2.0 Array (Affymetrix) and normalized by standard robust multichip average procedure. A single probe set of the highest variance among samples was chosen to represent *CD20* (228592_at; MS4A1) and *Ig* (211430_s_at; IGHG1, IGHG2, IGHV4-31, IGHM), respectively. To ensure data consistency, results from

additional probe sets were compared with a single probe set. Median value was used to calculate fold change of expression in tumor tissue compared with normal tissue. Statistical analyses were performed using the Wilcoxon rank-sum test to compare mRNA expression levels to their corresponding normal tissue controls.

Immunohistochemistry and Immunofluorescence

Detailed procedures are provided in the Supplementary Methods.

Cell Lines

Ink4 2.2 and *p53 2.1.1* cell lines were derived from primary PDAC tumors (FVB/N) of male transgenic *Pdx-Cre; LSL-Kras^{G12D}* mice harboring null mutations in *Trp53* and *Trp16^{Ink4a}* (10–16). Passage 3 of the cell lines was obtained in 2011 directly from the Hanahan laboratory, where they were derived and initially expanded. mCherry transfectants were expanded and frozen at low passage for use in the Coussens and Varner labs. Cells used in these studies were authenticated by gene expression in 2012 (RNA sequencing), whole exome analysis (in 2015), and BTK inhibitor sensitivity analyses (2013). All cell lines were tested for *Mycoplasma* contamination and grown in DMEM/10% FBS/1.0% penicillin and streptomycin on plastic coated with 50 μg/mL rat tail collagen I (BD Biosciences).

Animal Husbandry and In Vivo Studies

All animal experiments were performed with approval from the Institutional Animal Care and Use Committees of the University of California, San Diego, or Oregon Health and Science University. Generation and characterization of B cell-deficient *JH^{-/-}* (deletion in the J segment of the Ig heavy-chain locus and hence expressing no IgM or IgG and having no mature B cells), *FcRγ^{-/-}*, and *p110γ^{-/-}* mice have been described previously (17, 18, 25). All mice used for orthotopic implantation of PDAC cells were male FVB/n, 7 to 12 weeks of age. Mice receiving monoclonal antibodies for cellular depletion and/or cytokine neutralization were administered i.p. αCD8 (2.43, BioXcell) was administered on days 15, 20, and 25 after implantation at 500 μg/mouse; and αCSF1 (clone, BioXcell) was administered at 1.0 mg/mouse on day 21 and 500 μg/mouse on day 26. PCI-32765 (BTKi) was delivered *ad libitum* in drinking water at 0.16% w/v in a 2.0% β-hydroxycyclodextrin (Sigma) solution beginning on day 18, and continued until the end of the study. Gemcitabine was administered i.v. at 15 mg/kg on days 18, 22, and 26 after implantation. Alternatively, FVB/n mice inoculated orthotopically with *p53 2.1.1* PDAC cells were treated from day 7 with PCI-32765 (0.016% w/v in 2.0% β-hydroxycyclodextrin *ad libitum* in drinking water) or TG100-115 (2.5 mg/kg i.p., b.i.d.) with or without gemcitabine (15 mg/kg on days 7, 10, 13, 16, 19, 22, and 25 after implantation). Prior to surgery, mice were anesthetized with isoflurane, and abdominal hair surrounding the surgical site were removed. A left abdominal flank incision (1.5 cm) was made, and spleen and adherent pancreas were exteriorized. PDAC cells (1.0 × 10³ cells), mixed with 50% Matrigel and 50% serum-free DMEM in a total volume of 30 μL, were injected orthotopically into the tail of the pancreas of syngeneic 7-to-12-week-old male mice using a 30-gauge insulin needle, resulting in the appearance of a fluid bleb. Pancreas and spleen were then returned to their original position within the peritoneal cavity, followed by suture of the peritoneum and stapling of the skin. Staples were removed 7 days later, and tumor growth was monitored *in situ* using a Vevo 2100 small animal ultrasound (Visual Sonics) at days 14 and 27 following implantation. PDAC tumors were quantitated with ultrasound based on area (mm²) of the largest face of the tumor and percent change from days 14 to 27 was graphed, by weight in grams, or morphometrically using serial hematoxylin and eosin (H&E)-stained tissue sections by evaluating tumor area every 500 μm through the entire tissue depth and calculating the average

tumor area/section. Tissues were formalin-fixed or frozen in Tissue-Tek Optimal Cutting Temperature (O.C.T.) medium for histologic analysis. RNA was isolated from tissues flash-frozen in liquid nitrogen using the methods described for macrophage polarization.

Peripheral Blood Analysis

Blood was collected via cardiac puncture at necropsy or by saphenous vein at specific time points during the study and placed into EDTA-coated tubes to prevent clotting. Complete blood count analysis was acquired on a Cell Dyn 3700 analyzer. Plasma was collected by spinning whole blood at 13,000 RPM for 5 minutes, then cell-free supernatant was collected and snap-frozen for later analysis.

ELISA

Plasma from mice was thawed and diluted at 1:10,000 for assay of Ig levels and specific isotype. Concentrations of Ig in mouse plasma were determined using a standard curve and ELISA reagents from Southern BioTech. Human IgG was analyzed via the Human IgG Subclass Profile Kit from Novex-Life Technologies. Human samples were courtesy of the Oregon Pancreas Tumor Registry (OPTR). Data are shown as the fold increase relative to tumor-naïve mice.

Statistical Considerations

For all *in vitro* studies, experiments were performed three or more times with 3 or more biological replicates per experiment group. *In vivo* experiments were performed at least twice, with 10 to 15 randomly assigned mice/group for orthotopic tumor studies in WT and p110 γ ^{-/-} mice, and in mice treated with vehicle, PCI-32765, and TG100-115. A sample size of 15 mice/group provided 80% power to detect a mean difference of 1 standard deviation (SD) between two groups (based on a two-sample *t* test with two-sided 5% significance level). Prior to statistical analyses, data were examined for possible outliers using the Grubbs test. Data were normalized to the standard where applicable. Significance testing was performed by one-way ANOVA with Tukey *post hoc* testing for multiple pairwise testing or by parametric or nonparametric Student *t* test as appropriate. A two-sample *t* test (two groups) and ANOVA (multiple groups) were used when data were normally distributed, and a Wilcoxon rank-sum test (two groups) when data were not. All mouse studies were randomized for treatment by imaging all mice at day 14 after implantation and equally distributing mice into appropriate groups based on tumor size so that all groups began with a similar mean average (10–11 mm²) prior to treatment. Blinded assignment of mice into treatment groups, tumor measurement, and tumor analysis was performed by coding mice with randomly assigned mouse numbers, with the key unknown to operators until experiments were completed. Treatment studies were further blinded to evaluate tumor growth in response to therapy by having one investigator implant the mice and treat them while another investigator performed imaging at the indicated time points.

Additional detailed methods can be found in the Supplementary Methods.

Disclosure of Potential Conflicts of Interest

M.A. Tempero reports receiving commercial research support from Pharmacyclics. J.A. Varner reports receiving a commercial research grant from Acerta LLC and is a consultant/advisory board member for the same. L.M. Coussens reports receiving a commercial research grant from Acerta Pharma and is a consultant/advisory board member for Pharmacyclics. No potential conflicts of interest were disclosed by the other authors.

Authors' Contributions

Conception and design: A.J. Gunderson, M.M. Kaneda, N.I. Affara, M.A. Tempero, J.A. Varner, L.M. Coussens

Development of methodology: A.J. Gunderson, M.M. Kaneda, T. Tsujikawa, N.I. Affara, S. Gorjestani, B.Y. Chang, J.A. Varner, L.M. Coussens

Acquisition of data (provided animals, acquired and managed patients, provided facilities, etc.): A.J. Gunderson, M.M. Kaneda, A.V. Nguyen, N.I. Affara, B. Ruffell, S. Gorjestani, G. Kim, B. Sheppard, B. Irving, J.A. Varner, L.M. Coussens

Analysis and interpretation of data (e.g., statistical analysis, biostatistics, computational analysis): A.J. Gunderson, M.M. Kaneda, T. Tsujikawa, A.V. Nguyen, N.I. Affara, B. Ruffell, S. Gorjestani, S.M. Liudahl, M.A. Tempero, J.A. Varner, L.M. Coussens

Writing, review, and/or revision of the manuscript: A.J. Gunderson, M.M. Kaneda, T. Tsujikawa, D. Hanahan, M.A. Tempero, B.Y. Chang, J.A. Varner, L.M. Coussens

Administrative, technical, or material support (i.e., reporting or organizing data, constructing databases): A.J. Gunderson, T. Tsujikawa, M. Truitt, P. Olson, D. Hanahan, J.A. Varner, L.M. Coussens

Study supervision: A.J. Gunderson, J.A. Varner, L.M. Coussens

Acknowledgments

The authors thank Xiaodan Song, Justin Tibbitts, Teresa Beechwood, Jo Hill, and Amy Li for regulatory and technical assistance; Jason Link for facilitating acquisition of human pancreas samples and HIPAA-compliant clinical data; Sushil Kumar and Terry Medler for helpful discussion; and support from the Knight Cancer Center Flow Cytometry, Bioinformatics, and Advanced Light Microscopy shared resources.

Grant Support

The authors acknowledge support from T32AI078903-04 to A.J. Gunderson; T32HL098062 to M.M. Kaneda; T32CA009523 and T32CA121938 to S. Gorjestani; R01CA167426-03S1 to A.V. Nguyen; support from the NCI/NIH (R01CA167426, R01CA126820, and R01CA083133) to J.A. Varner; and support from the NCI/NIH (R01CA130980, R01CA140943, R01CA15531, and U54CA163123), the Department of Defense Breast Cancer Research Program (W81XWH-11-1-0702), the Susan G. Komen Foundation (KG110560 and KG111084), the Brenden-Colson Center for Pancreatic Health, and a Stand Up To Cancer–Lustgarten Foundation Pancreatic Cancer Convergence Dream Team Translational Research Grant (SU2C-AACR-DT14-14) to L.M. Coussens. Stand Up To Cancer is a program of the Entertainment Industry Foundation administered by the American Association for Cancer Research.

Received July 08, 2015; revised December 14, 2015; accepted December 22, 2015; published OnlineFirst December 29, 2015.

REFERENCES

- Hanahan D, Coussens LM. Accessories to the crime: functions of cells recruited to the tumor microenvironment. *Cancer Cell* 2012;21:309–22.
- Schmid MC, Varner JA. Myeloid cells in tumor inflammation. *Vasc Cell* 2012;4:14.
- Coussens LM, Zitvogel L, Palucka AK. Neutralizing tumor-promoting chronic inflammation: a magic bullet? *Science* 2013;339:286–91.
- SEER.cancer.gov [Internet]. Rockville: National Cancer Institute; c2015. Available from: <http://seer.cancer.gov/statfacts/html/pancreas.html>.
- Siegel R, Naishadham D, Jemal A. Cancer statistics, 2012. *CA Cancer J Clin* 2012;62:10–29.

6. Conroy T, Desseigne F, Ychou M, Bouche O, Guimbaud R, Becouarn Y, et al. FOLFIRINOX versus gemcitabine for metastatic pancreatic cancer. *N Engl J Med* 2011;364:1817–25.
7. Von Hoff DD, Ramanathan RK, Borad MJ, Laheru DA, Smith LS, Wood TE, et al. Gemcitabine plus nab-paclitaxel is an active regimen in patients with advanced pancreatic cancer: a phase I/II trial. *J Clin Oncol* 2011;29:4548–54.
8. Shibuya KC, Goel VK, Xiong W, Sham JG, Pollack SM, Leahy AM, et al. Pancreatic ductal adenocarcinoma contains an effector and regulatory immune cell infiltrate that is altered by multimodal neoadjuvant treatment. *PLoS One* 2014;9:e96565.
9. Affara NI, Ruffell B, Medler TR, Gunderson AJ, Johansson M, Bornstein S, et al. B cells regulate macrophage phenotype and response to chemotherapy in squamous carcinomas. *Cancer Cell* 2014;25:809–21.
10. Jackson EL, Willis N, Mercer K, Bronson RT, Crowley D, Montoya R, et al. Analysis of lung tumor initiation and progression using conditional expression of oncogenic K-ras. *Genes Dev* 2001;15:3243–8.
11. Hingorani SR, Petricoin EF, Maitra A, Rajapakse V, King C, Jacobetz MA, et al. Preinvasive and invasive ductal pancreatic cancer and its early detection in the mouse. *Cancer Cell* 2003;4:437–50.
12. Tuveson DA, Shaw AT, Willis NA, Silver DP, Jackson EL, Chang S, et al. Endogenous oncogenic K-ras(G12D) stimulates proliferation and widespread neoplastic and developmental defects. *Cancer Cell* 2004;5:375–87.
13. Sharpless NE, Bardeesy N, Lee KH, Carrasco D, Castrillon DH, Aguirre AJ, et al. Loss of p16Ink4a with retention of p19Arf predisposes mice to tumorigenesis. *Nature* 2001;413:86–91.
14. Marino S, Vooijs M, van Der Gulden H, Jonkers J, Berns A. Induction of medulloblastomas in p53-null mutant mice by somatic inactivation of Rb in the external granular layer cells of the cerebellum. *Genes Dev* 2000;14:994–1004.
15. Bardeesy N, Aguirre AJ, Chu GC, Cheng KH, Lopez LV, Hezel AF, et al. Both p16(Ink4a) and the p19(Arf)-p53 pathway constrain progression of pancreatic adenocarcinoma in the mouse. *Proc Natl Acad Sci U S A* 2006;103:5947–52.
16. Gu G, Dubauskaite J, Melton DA. Direct evidence for the pancreatic lineage: NGN3+ cells are islet progenitors and are distinct from duct progenitors. *Development* 2002;129:2447–57.
17. Chen J, Trounstein M, Alt FW, Young F, Kurahara C, Loring JF, et al. Immunoglobulin gene rearrangement in B cell deficient mice generated by targeted deletion of the JH locus. *Int Immunol* 1993;5:647–56.
18. Takai T, Li M, Sylvestre D, Clynes R, Ravetch JV. FcR gamma chain deletion results in pleiotropic effector cell defects. *Cell* 1994;76:519–29.
19. Andreu P, Johansson M, Affara NI, Pucci F, Tan T, Junankar S, et al. FcRgamma activation regulates inflammation-associated squamous carcinogenesis. *Cancer Cell* 2010;17:121–34.
20. Ruffell B, Chang-Strachan D, Chan V, Rosenbusch A, Ho CM, Pryer N, et al. Macrophage IL-10 blocks CD8+ T cell-dependent responses to chemotherapy by suppressing IL-12 expression in intratumoral dendritic cells. *Cancer Cell* 2014;26:623–37.
21. de Gorter DJ, Beuling EA, Kersseboom R, Middendorp S, van Gils JM, Hendriks RW, et al. Bruton's tyrosine kinase and phospholipase Cgamma2 mediate chemokine-controlled B cell migration and homing. *Immunity* 2007;26:93–104.
22. Hendriks RW, Yuvaraj S, Kil LP. Targeting Bruton's tyrosine kinase in B cell malignancies. *Nat Rev Cancer* 2014;14:219–32.
23. DeNardo DG, Brennan DJ, Rexhepaj E, Ruffell B, Shiao SL, Madden SF, et al. Leukocyte complexity predicts breast cancer survival and functionally regulates response to chemotherapy. *Cancer Discov* 2011;1:54–67.
24. Schmid MC, Franco I, Kang SW, Hirsch E, Quilliam LA, Varner JA. PI3-kinase gamma promotes Rap1a-mediated activation of myeloid cell integrin alpha4beta1, leading to tumor inflammation and growth. *PLoS One* 2013;8:e60226.
25. Schmid MC, Avraamides CJ, Dippold HC, Franco I, Foubert P, Ellies LG, et al. Receptor tyrosine kinases and TLR/IL1Rs unexpectedly activate myeloid cell PI3Kgamma, a single convergent point promoting tumor inflammation and progression. *Cancer Cell* 2011;19:715–27.
26. Schmid MC, Avraamides CJ, Foubert P, Shaked Y, Kang SW, Kerbel RS, et al. Combined blockade of integrin-alpha4beta1 plus cytokines SDF-1alpha or IL-1beta potently inhibits tumor inflammation and growth. *Cancer Res* 2011;71:6965–75.
27. Dangi-Garimella S. FDA grants accelerated approval for ibrutinib for CLL. *Am J Manag Care* 2014;20:SP145.
28. Palanki MS, Dneprovskaia E, Doukas J, Fine RM, Hood J, Kang X, et al. Discovery of 3,3'-(2,4-diaminopteridine-6,7-diyl)diphenol as an isozyme-selective inhibitor of PI3K for the treatment of ischemia reperfusion injury associated with myocardial infarction. *J Med Chem* 2007;50:4279–94.
29. Bonecchi R, Sozzani S, Stine JT, Luini W, D'Amico G, Allavena P, et al. Divergent effects of interleukin-4 and interferon-gamma on macrophage-derived chemokine production: an amplification circuit of polarized T helper 2 responses. *Blood* 1998;92:2668–71.
30. Biswas SK, Gangi L, Paul S, Schioppa T, Saccani A, Sironi M, et al. A distinct and unique transcriptional program expressed by tumor-associated macrophages (defective NF-kappaB and enhanced IRF-3/STAT1 activation). *Blood* 2006;107:2112–22.
31. Benson MJ, Rodriguez V, von Schack D, Keegan S, Cook TA, Edmonds J, et al. Modeling the clinical phenotype of BTK inhibition in the mature murine immune system. *J Immunol* 2014;193:185–97.
32. Pylayeva-Gupta Y, Lee KE, Hajdu CH, Miller G, Bar-Sagi D. Oncogenic Kras-induced GM-CSF production promotes the development of pancreatic neoplasia. *Cancer Cell* 2012;21:836–47.
33. Keenan BP, Saenger Y, Kafrouni MI, Leubner A, Lauer P, Maitra A, et al. A Listeria vaccine and depletion of T-regulatory cells activate immunity against early stage pancreatic intraepithelial neoplasms and prolong survival of mice. *Gastroenterology* 2014;146:1784–94e6.
34. Beatty GL, Chiorean EG, Fishman MP, Saboury B, Teitelbaum UR, Sun W, et al. CD40 agonists alter tumor stroma and show efficacy against pancreatic carcinoma in mice and humans. *Science* 2011;331:1612–6.
35. Twyman-Saint Victor C, Rech AJ, Maity A, Rengan R, Pauken KE, Stelekati E, et al. Radiation and dual checkpoint blockade activate non-redundant immune mechanisms in cancer. *Nature* 2015;520:373–7.
36. Sagiv-Barfi I, Kohrt HE, Czerwinski DK, Ng PP, Chang BY, Levy R. Therapeutic antitumor immunity by checkpoint blockade is enhanced by ibrutinib, an inhibitor of both BTK and ITK. *Proc Natl Acad Sci U S A* 2015;112:E966–72.
37. Masso-Valles D, Jauset T, Serrano E, Sodir NM, Pedersen K, Affara NI, et al. Ibrutinib exerts potent antifibrotic and antitumor activities in mouse models of pancreatic adenocarcinoma. *Cancer Res* 2015;75:1675–81.
38. Schioppa T, Moore R, Thompson RG, Rosser EC, Kulbe H, Nedospasov S, et al. B regulatory cells and the tumor-promoting actions of TNF-alpha during squamous carcinogenesis. *Proc Natl Acad Sci U S A* 2011;108:10662–7.
39. Wong SC, Puaux AL, Chittezhath M, Shalova I, Kajiji TS, Wang X, et al. Macrophage polarization to a unique phenotype driven by B cells. *Eur J Immunol* 2010;40:2296–307.
40. Woo JR, Liss MA, Muldong MT, Palazzi K, Strasner A, Ammirante M, et al. Tumor infiltrating B-cells are increased in prostate cancer tissue. *J Transl Med* 2014;12:30.
41. Ammirante M, Luo JL, Grivennikov S, Dedospasov S, Karin M. B-cell-derived lymphotoxin promotes castration-resistant prostate cancer. *Nature* 2010;464:302–6.
42. Shalapour S, Font-Burgada J, Di Caro G, Zhong Z, Sanchez-Lopez E, Dhar D, et al. Immunosuppressive plasma cells impede T-cell-dependent immunogenic chemotherapy. *Nature* 2015;521:94–8.
43. Inoue S, Leitner WW, Golding B, Scott D. Inhibitory effects of B cells on antitumor immunity. *Cancer Res* 2006;66:7741–7.
44. Pylayeva-Gupta Y, Das S, Handler JS, Hajdu CH, Coffre M, Koralov S, et al. IL35-producing B cells promote the development of pancreatic neoplasia. *Cancer Discov* 2016;6:247–55.

45. Lee KE, Spata M, Bayne LJ, Buza EL, Durham AC, Allman D, et al. *HIF1 α* deletion reveals pro-neoplastic function of B cells in pancreatic neoplasia. *Cancer Discov* 2016;6:256–69.
46. Sistiug A, Yamazaki T, Vacchelli E, Chaba K, Enot DP, Adam J, et al. Cancer cell-autonomous contribution of type I interferon signaling to the efficacy of chemotherapy. *Nat Med* 2014;20:1301–9.
47. Xue J, Sharma V, Hsieh MH, Chawla A, Murali R, Pandol SJ, et al. Alternatively activated macrophages promote pancreatic fibrosis in chronic pancreatitis. *Nat Commun* 2015;6:7158.
48. Lemos DR, Babaeijandaghi F, Low M, Chang CK, Lee ST, Fiore D, et al. Nilotinib reduces muscle fibrosis in chronic muscle injury by promoting TNF-mediated apoptosis of fibro/adipogenic progenitors. *Nat Med* 2015;21:786–94.
49. Lin EY, Nguyen AV, Russell RG, Pollard JW. Colony-stimulating factor 1 promotes progression of mammary tumors to malignancy. *J Exp Med* 2001;193:727–40.
50. DeNardo DG, Barreto JB, Andreu P, Vasquez L, Tawfik D, Kolhatkar N, et al. CD4(+) T cells regulate pulmonary metastasis of mammary carcinomas by enhancing protumor properties of macrophages. *Cancer Cell* 2009;16:91–102.
51. Gocheva V, Wang HW, Gadea BB, Shree T, Hunter KE, Garfall AL, et al. IL-4 induces cathepsin protease activity in tumor-associated macrophages to promote cancer growth and invasion. *Genes Dev* 2010;24:241–55.

CANCER DISCOVERY

Bruton Tyrosine Kinase–Dependent Immune Cell Cross-talk Drives Pancreas Cancer

Andrew J. Gunderson, Megan M. Kaneda, Takahiro Tsujikawa, et al.

Cancer Discov 2016;6:270-285. Published OnlineFirst December 29, 2015.

Updated version Access the most recent version of this article at:
doi:[10.1158/2159-8290.CD-15-0827](https://doi.org/10.1158/2159-8290.CD-15-0827)

Supplementary Material Access the most recent supplemental material at:
<http://cancerdiscovery.aacrjournals.org/content/suppl/2015/12/24/2159-8290.CD-15-0827.DC1.html>

Cited articles This article cites 49 articles, 19 of which you can access for free at:
<http://cancerdiscovery.aacrjournals.org/content/6/3/270.full.html#ref-list-1>

Citing articles This article has been cited by 1 HighWire-hosted articles. Access the articles at:
<http://cancerdiscovery.aacrjournals.org/content/6/3/270.full.html#related-urls>

E-mail alerts [Sign up to receive free email-alerts](#) related to this article or journal.

Reprints and Subscriptions To order reprints of this article or to subscribe to the journal, contact the AACR Publications Department at pubs@aacr.org.

Permissions To request permission to re-use all or part of this article, contact the AACR Publications Department at permissions@aacr.org.

Bruton's Tyrosine Kinase (BTK)-dependent immune cell crosstalk drives pancreas cancer

Andrew J. Gunderson^{1,14}, Megan M. Kaneda^{5,14}, Takahiro Tsujikawa^{1,2}, Abraham Nguyen⁵, Nesrine I. Affara⁷, Brian Ruffell¹, Sara Gorjestani⁵, Shannon M. Liudahl¹, Morgan Truitt⁹, Peter Olson⁹, Grace Kim^{7,10}, Douglas Hanahan⁶, Margaret Tempero^{8,10}, Brett Sheppard^{3,4}, Bryan Irving¹¹, Betty Y. Chang¹², Judith A. Varner^{5,13,14}, Lisa M. Coussens^{1,4,14,#}

SUPPLEMENTARY METHODS

Immunohistochemistry and Immunofluorescence: Brightfield immunodetection studies using human tissue sections was performed as described previously (1). De-identified human tissue was received from the University of California, San Francisco (UCSF) Department of Pathology under approval from the UCSF Committee on Human Research (05028310), and the Oregon Health and Science University (OHSU) Oregon Pancreas Tumor Registry (OPTR) and courtesy of Dr. Brett Sheppard (institutional review board [IRB] #3609), with patient consent obtained prior to tissue acquisition. The use of samples occurred under “exempt category 4” for individuals receiving de-identified biological specimens. Antibodies used were: α CD45 (H130, 1:500, eBioscience), α CD20 (L26, 1:100, Abcam), α CD3 ϵ (SP7, 1:200, Thermo Scientific), α CD8 (C8/144B, 1:100, Thermo Scientific).

IHC was conducted with FFPE (5 μ m) tissue sections of human PDAC subjected to heat-mediated antigen retrieval immersed in citrate buffer (pH 6.0) for 15 min. prior to blocking with 5% goat serum for 30 min. For human IHC, primary murine or rabbit antibodies were then serially stained for 2 hours at RT or O/N at 4° C using mouse anti-CD20 (L-26, 1:100, Santa Cruz), mouse anti-CD8 (C8/144B, 1:100; Thermo Scientific), Rabbit anti-CD3 (SP7, 1:200, Thermo Scientific), mouse anti-CD45 (30-F11, 1:100, eBioscience), rabbit anti-CD11b (1:1000, Abcam), , and rabbit anti-BTK (D3H5, 1:100, Cell Signaling). Following washing of each antibody, primary antibodies were stained with either an anti-mouse or anti-rabbit Histofine Simple Stain MAX PO HRP conjugated polymer (Nichirei Biosciences Inc.) for 30 min. at RT followed by DAB (singleplex) or AEC (multiplex) for peroxidase detection. Slides were scanned at Aperio ImageScope AT (Leica Biosystems) at either 20x (multiplex) or 40x (singleplex) magnification. Samples chosen for multiplex staining were destained in an alcohol gradient following the whole slide scanning and image processing according to a protocol of Glass et. al., (2). Slides were restained sequentially with the indicated antibodies following the antibody stripping protocol in heat retrieval as reported (3). Multiplex images were coregistered using CellProfiler software (Broad Institute), deconvoluted using Image J, pseudocolored and merged in ImageScope (Aperio, Leica). High magnification images were created with a 5x zoom from a 20x original magnification. For murine IHC, immunodetection of murine tissue sections was performed as previously described (4). Antibodies used were as follows: α B220 (RA3-6B2, 1:500, BD Biosciences), α BrdU (MCA2060, 1:2000 AbD Serotec), α CC3 (D175, 1:500, Cell Signaling), α CD11b (M1/70, 1:200, BD Biosciences), α CD8a (53-6.7, 1:50, BD Biosciences), α CD31 (MEC13.3, 1:500, BD Biosciences), α Granzyme B (NB100-684, 1:100, Novus Biologicals), and α SMA (ab5694, 1:250, Abcam). Analysis of positive staining was achieved utilizing Aperio automated scanning (Leica) and IHC quantitation software (ScanScope).

Flow cytometry: Single cell suspensions from blood, spleen, and peritoneal cavity were prepared as previously described (4). Mouse and human tumor tissue was collected and stored in PBS/0.1% soybean trypsin inhibitor prior to enzymatic

dissociation. Mice were cardiac-perfused with 10-15 ml PBS/10 u/ml heparin prior to collection to clear peripheral blood. Samples were finely minced with a scissors and mouse tissue was transferred into DMEM containing 1.0 mg/ml collagenase IV (Gibco), 0.1% soybean trypsin inhibitor, and 50 U/ml DNase (Roche) and incubated at 37°C for 30 min. with constant stirring while human tissue was digested in 2.0 mg/ml collagenase IV, 1.0 mg/ml hyaluronidase, 0.1% soybean trypsin inhibitor, and 50 U/ml DNase for 45 minutes. Suspensions were filtered through a 100 micron filter and washed with FACS buffer (PBS/0.5% BSA/2.0 mM EDTA) prior to staining. Two million total cells were stained with antibodies as indicated. Intracellular detection of pBTK (Y223) and cytokines was achieved following permeabilization with BD Perm Buffer III (BD Biosciences) and eBioscience Fix/Perm respectively. Intracellular detection of cytokines occurred following *ex vivo* stimulation of cells in complete RPMI media containing 50 ng/ml PMA, 500 ng/ml Ionomycin, 2.0 µM Monensin (BD Biosciences) and 1.0 µg/ml LPS. Following staining, samples were acquired on a BD Fortessa or LSRII (BD Biosciences) and analyzed using FlowJo (Treestar) software. Antibodies used for murine FACS were as follows: CD4 (RM4-5, 1:400, Biolegend), CD8 (53-6.7, 1:400, Biolegend), CD19 (6D5, 1:400, Biolegend), B220 (RA3-6B2, 1:400, Biolegend), MHCII (M5/114.15.2, 1:1000, eBioscience), Gr-1 (RB6-8C5, 1:400, eBioscience), Ly6G (1A8, 1:400, eBioscience), Ly6C (HK1.4, 1:400, Biolegend), F4/80 (BM8, 1:400, Biolegend), CD11c (N418, 1:400, eBioscience), CD3 (17A2, 1:200, Biolegend), IL-10 (JES5-16E3, 1:200, eBioscience), CD5 (53-7.3, 1:400, eBioscience), CD1d (1B1, 1:400, BD Biosciences), CD45 (30-F11, 1:4000, eBioscience), Granzyme B (NGZB, 1:200, eBioscience), CD64 (X54-5/7.1, 1:200, Biolegend), CD16/CD32 (93, 1:200, Biolegend), Foxp3 (FJK-16s, 1:400, eBioscience), and pBTK-Y223 (N35-86, 1:400, BD Biosciences), EOMES (Dan11mag, 1:400, eBioscience), PD-1 (RMP1-30, 1:400, Biolegend), CD107a (1D4B, 1:200, Biolegend), IFN-γ (XMG1.2, 1:400, eBioscience), CD138 (281-2, 1:400, BD Bioscience), CD23 (B3B4, 1:800, eBioscience), and IgM (II/41, 1:400, eBioscience). Antibodies used for human FACS were as follows: CD45 (2D1, 1:100, BD Biosciences), CD4 (1:50, OKT4, Biolegend), CD8 (RPA-T8, 1:100, Biolegend), CD19 (HIB19, 1:100, BD Biosciences), HLA-DR (L243, 1:100, eBioscience), CD11c (3.9, 1:200, eBiosciences), CD11b (ICRF44, 1:200, Biolegend), CD15 (HI98, 1:200, Biolegend), CD14 (HCD14, 1:50, Biolegend), CD206 (19.2, 1:100, BD Biosciences), FoxP3 (236A/E7, 1:50, eBioscience), CD3 (OKT3, 1:50, eBioscience), FcεR1α (AEP-37, 1:50, eBioscience), and CD117 (YB5.B8, 1:50, BD Biosciences). CD64 (X54-5/7.1, 1:100, BD Biosciences), and CD16 (3G8, 1:100, Biolegend).

Real-time PCR: Mice were cardiac-perfused with PBS to clear peripheral blood. Following enzymatic digestion as previously described (4), leukocyte subsets were isolated from tissue by FACS using an Influx Cell Sorter or Aria II (BD Biosciences) as previously described (4), and collected directly into RLT lysis buffer for subsequent RNA extraction using RNeasy Micro/Mini kit guidelines (Qiagen). Contaminating DNA was removed with DNase I (Invitrogen). SuperScript III (Invitrogen) was used to reverse transcribe purified RNA into cDNA according to manufacturer's directions. Real-time PCR for gene expression was performed using the TaqMan system (Applied Biosystems) with a 14 cycle preamplification step employed during analysis of FACS-sorted populations. The comparative threshold cycle method was used to calculate fold change in gene expression, which was normalized to *Gapdh* and TATA-binding protein (*Tbp*) as reference genes. For TG100-115 and PCI-32765 tumor studies, qPCR was performed using custom PrimePCR plates (Biorad), where mRNA levels were normalized to *gapdh* as reference gene.

Splenocyte stimulation: Splenic single cell suspensions were harvested from tumor naïve FVB/n male mice and subjected to *in vitro* stimulation with 10 µg/ml αIgM F(ab)[']2 fragment for 2 minutes or 25 µg/ml αCD16/CD32 for 10 minutes on ice followed by F(ab)[']2 fragment goat anti-rat IgG Fc specific (Jackson Immunolaboratories) for 5 minutes in serum free RPMI media. Following stimulation, cells were washed with PBS/0.5% BSA/2.0 mM EDTA supplemented with phosphatase inhibitors and FACS stained for Live/Dead Aqua (Invitrogen), CD3-APC, CD19-Brilliant Violet 650, CD11b-FITC and MHCII-EFluor450 for 30 min. Cells were then fixed with BD Cytofix (BD Biosciences) for 20 minutes. Fixative was washed off with PBS and cells were permeabilized with BD Perm Buffer III for 30 minutes on ice. Upon removal of permeabilization buffer, cells were stained with anti-pBTK (Y223)-PE for 30 minutes and acquired on a BD Fortessa.

Bone Marrow-derived macrophage isolation and gene expression analysis: Bone marrow was harvested by perfusing femurs of 7-12 week old FcRγ^{+/-} male mice with DMEM 10% FBS/1.0% Pen/Strep into plastic culture dishes. Suspensions were filtered through a 70-micron mesh, washed 1x and resuspended in RBC lysis buffer to remove contaminating red blood cells. Following wash of RBC lysis, cells were counted and plated in DMEM 10% FBS/1.0% Pen/Strep/10 ng/ml CSF-1 (PeproTech) at a density of 1 x10⁵ cells/ml. Following three days in culture, 50% of the medium was exchanged with fresh complete DMEM with 20 ng/ml CSF-1. After 2 days, cells were visualized to confirm morphological presence of macrophages and one well counted and stained for FACS analysis to ensure macrophage differentiation. If necessary, cells were cultured for one or two more days in fresh complete medium to achieve the desired number of cells for study. Alternatively, bone marrow-derived macrophages were generated from C57BL/6, BTK^{-/-} or p110γ^{-/-} mice as described above and polarized with IFN-γ (20 ng/ml, PeproTech)/LPS (100 ng/ml, Sigma) for 24 hours or IL-4 (20 ng/ml, PeproTech) for 48 hours. In some studies, macrophages polarized with IL-4 for 24 h were incubated with purified rat anti-mouse CD16/CD32 (BD Pharmingen) at 1.0 µg/10⁶ cells for 10 min 4°C and then incubated with goat anti-rat F(ab)[']2 (25 µg/ml, Jackson ImmunoResearch) for 24 hour. Total RNA was harvested from macrophages using the RNeasy Mini Kit (Qiagen) according to the manufacturer's instructions and cDNA was prepared using 1.0 µg RNA with the qScript cDNA Synthesis Kit (Quanta Biosciences). Sybr green based qPCR was performed using murine primers to *Arg1*, *Il10*, *Ccl2*, *Mmp9*, *Il12p40*, *Il1b*, *Il6*, *Gapdh*, *Nos2*, *p110g*, *p110d*, *Btk*, *Plcg2* and *Tnfa* from Qiagen (QuantiTect Primer sets, Qiagen). mRNA levels were normalized to Gapdh levels (dCt = Ct gene of interest – Ct Gapdh) and reported as either relative mRNA expression (ddCt = 2^(dCt sample – dCt control)) or as fold change (fold change = log₂(dCt test / dCt control) with n=3).

Immunoblotting: Macrophages, B cells and in vitro cultured p53 2.1.1 or Ink4a 2.2.1 PDAC cells were solubilized in RIPA buffer containing protease and phosphatase inhibitors. Proteins were separated by gradient gel electrophoresis, electrophoretically transferred to PVDF membranes. PVDF membranes were immunoblotted with antibodies from Cell Signaling: α-Btk (C82B8), α-p110γ (4252), α-p110α (4255), δ-p110δ (100-401-862, Rockland), α-pBTK (clone EP420Y, Epitomics), or α-actin (A2103, Sigma-Aldrich).

Cell Proliferation Assay: Macrophages and in vitro cultured p53 2.1.1 or Ink4a 2.2.1 PDAC cells were plated in 96 well plates and treated with dilutions of PCI-32765, TG100-115 (Targegen, Inc., La Jolla, CA) or DMSO (vehicle control) for

72h (n=3). Thiazolyl blue tetrazolium bromide (5.0 mg/ml, Sigma) was incubated with cells and solubilized with DMSO. Absorbance was determined at 560 nm.

Cell adhesion and integrin activation assays

siRNA transfections: CD11b⁺ cells were purified from BM by anti-CD11b magnetic bead affinity chromatography according to manufacturer's directions (130-049-601, Miltenyi Biotec). Purified CD11b⁺ cells or primary murine macrophages were transfected with 100 nM of *Btk* (Mm_Btk_1 and Mm_Btk_2) or *Plcg2* (Mm_Plcg 2_1 and Mm_Plcg2_5) siRNA or with plasmids + pGFPMax using an AMAXA Mouse Macrophage Nucleofection Kit (VAPA-1009, as previously described (5)). After transfection, cells were cultured for 48 h in media containing 20% serum prior to evaluation of cell adhesion or gene expression. At least two siRNA/per gene were tested individually for efficient knockdown of protein expression and for inhibition of adhesion or gene expression.

Adhesion assays: 1.0×10^5 calcein-AM labeled CD11b⁺ cells were incubated on HUVEC monolayers or plastic plates coated with 5.0 µg/ml recombinant soluble VCAM-1 (643-VM-050, R&D Systems) in the absence or presence of dilutions of PCI-32765 or TG100-115 or corresponding dilutions of DMSO for 30 minutes at 37°C with humidity in the presence of DMEM containing 200 ng/ml SDF-1α or IL-1β (R&D Systems) as previously described (5). After washing three times with warmed medium, adherent cells were quantified using a plate fluorimeter (GeniosPro, TECAN).

Ligand (VCAM-1) binding assay: 5×10^5 murine bone marrow derived CD11b⁺ cells were incubated with DMEM, 200ng/ml SDF-1α in DMEM, or DMEM containing DMSO or 1.0 µM PCI-32765 together with 1.0 mg/ml mouse VCAM-1/human Fc fusion protein (643-VM-050, R&D Systems) for 3 min. Cells were washed twice and incubated with donkey anti-human-Fcγ₁-PE antibody (709-116-098, Jackson ImmunoResearch), fixed and analysed by FACS Calibur. Mean fluorescence intensity of treated cells was compared to that of unstimulated cells (basal).

In vitro macrophage B cell co-culture: Bone marrow derived macrophages were plated in the lower chamber of 24 well co-culture chamber plates in the presence of basal or p53 2.1.1 tumor cell conditioned medium. CD19⁺ cells were purified by magnetic bead isolation from single cell splenic preparations of d14 p53 2.1.1 tumor bearing mice (CD19 MACS Microbeads, Miltenyi Biotec). Cells were washed with PBS and added to the upper chamber of co-culture chambers (12 mm diameter Millicell Cell Culture Insert, Millipore) at a ratio of 3:1 B cells to macrophages respectively and incubated for 24h at 37°C/5% CO₂. For inhibitor treated conditions, CD19⁺ cells were incubated with 1.0 µM PCI-32165 for 30 min at 37°C/5% CO₂.

In vivo macrophage and B cell adoptive transfer experiment: CD11b⁺Gr1⁻ cells were isolated from single cell suspensions of WT p53 2.1.1 tumors. CD19⁺ cells were isolated from single cell splenic preparations from d14 tumor bearing mice by magnetic bead isolation. Purified cells were mixed 1:1 for CD11b⁺Gr1⁻ cells or 1:5 for CD19⁺ cells with p53 2.1.1 tumor cells, and 5×10^5 total tumor cells were injected into host mice. For inhibitor treated groups, CD11b⁺Gr1⁻ or CD19⁺ cells were incubated with 1.0 µM PCI-32765 for 30 min before the addition of tumor cells. Inoculated mice were further treated by intradermal injections of PCI-32765 at 3 and 6 days post inoculation and mice were sacrificed and tumor weights were determined.

Mast cell quantitation: Mast cells were identified by 0.1% Toluidine blue (1% w/v NaCl, pH 2.3) staining of FFPE

tissue sections for 2 min., followed by an alcohol destaining process. Following staining, mast cells were identified by their purple metachromasia and degranulated mast cells were identified by appearance of punctate granules loosely arranged within the cytoplasm and pericellular space. Percent of degranulated mast cells was calculated by dividing the number of degranulated mast cells by the total number of mast cells within in a given tissue section.

SUPPLEMENTARY FIGURE LEGENDS

Supplementary Figure S1. B cells in human PDAC. **A.** mRNA expression of *CD20* (*MS4A1*), *IgG1* (*IGHG1*), *IgG3* (*IGHG3*), and *IgM* (*IGHM*) in human PDAC tumors (blue) versus healthy (pink) pancreas analyzed from RNA sequence data compiled from the Oncomine database. Data are represented as box-and-whisker plots depicting median fold change value compared to normal tissue, displaying the first and third quartiles at the end of each box, with the maximum and minimum at the ends of the whiskers. 39 PDAC patients and 39 healthy controls were assessed in each graph. **B.** IgG levels in human plasma from patients with various pancreas neoplasms versus healthy controls as determined via ELISA. Healthy, n = 6; PDAC, n = 13; IPMN, n = 12; pancreatitis, n = 10; PNET, n = 5. Data are represented as box-and-whisker plots depicting median fold change value compared to normal tissue, displaying the first and third quartiles at the end of each box, with the maximum and minimum at the ends of the whiskers. **C.** FACS gating strategy for single cell suspensions from primary human PDAC tissue collected following surgical resection. **D.** Shown are representative FACS quantitation of individual cell populations representing complexity analysis of populations shown in Fig. 1C.

Supplementary Figure S2. B cells and FcR γ -positive cells regulate murine PDAC. **A.** Photomicrographs of end-stage orthotopic Ink4 2.2, and p53 2.1.1 PDAC tumor sections, as compared to transgenic KIC and KPC PDAC tumors sections stained for B220. **B and C.** Representative photomicrographs of Ink4 2.2 and p53 2.1.1-derived orthotopic PDAC tumors from end-stage mice from syngeneic JH^{+/+}, JH^{-/-} (**B**), FcR γ ^{+/+} and FcR γ ^{-/-} (**C**) mice. Shown are representative H&E and Gomori trichrome-stained FFPE tissue sections. **D.** FACS gating strategy for single cell suspensions from primary mouse PDAC tissue collected at necropsy. **E.** FACS analysis of B cell subsets day 28 end-stage Ink4 2.2 PDAC tumors following no treatment, PCI-32765 alone, Gem alone, or Gem + PCI-32765. B cell subsets were identified and gated based on the following markers: total B cells: CD45⁺CD19⁺CD3⁻, Bregs: CD5⁺CD1d^{hi}, Plasma Cells: CD138⁺IgM^{lo}, Plasma Blasts: CD138⁺IgM^{hi}, B1a: IgM^{hi}CD23⁻CD5⁺, B1b: IgM^{hi}CD23⁻CD5⁻CD1d^{lo}, Marginal Zone (Mz) B: IgM^{hi}CD23⁻CD5⁻CD1d^{hi}, Follicular B: IgM^{lo}CD23⁺CD5⁻. All B cell subsets were gated as a percentage of total CD19⁺ B cells. Data from two independent experimental studies is shown. Statistical significance was determined using the student's T test with * reflecting p values <0.05. **F.** FACS analysis of single cell suspensions reflecting cell types shown, isolated from Ink4 2.2-derived PDAC (n=5 mice) at end-stage and stained for Fc γ R1 (CD64) and Fc γ RII/III (CD16/CD32). Data are background subtracted from MFI of counterpart cells from FcR γ ^{-/-} tumor bearing mice and reflective of 2 independent experiments. **G.** FACS analysis of single cell suspensions reflecting cell types shown, isolated from Ink4 2.2-derived PDAC grown in FcR γ ^{+/+} versus FcR γ ^{-/-} mice at end-stage and stained for Fc γ R1 (CD64) and Fc γ RII/III (CD16/CD32). Data are reflective of 2 independent experiments.

Supplementary Figure S3. Leukocytes and BTK in human and murine PDAC. **A.** Composite photomicrograph showing immunoreactivity for CD45 (light green), CD20 (white), CSF-1R (light blue), CD11b (red), BTK (orange), and DNA (dark blue) in a human PDAC FFPE tissue section. **B.** Phosphorylation (Y223) levels of murine BTK in B cell receptor (BCR)- (α IgM) or Fc γ R- (α CD16/CD32) stimulated naïve splenocytes as measured by FACS and displayed as mean fluorescent intensity (MFI) between the indicated leukocyte populations. Groups were assayed in triplicate in two independent experiments. **C.** Percent change in growth of Ink4 2.2 PDACs in syngeneic mice following administration

of Gem, α CSF1-neutralizing mAb (clone 5A1), or Gem and α CSF1 as depicted by treatment shown in Fig. 6A. Quantitation of macrophage depletion by FACS of single cell suspensions from PDAC tumors from treatment groups as shown. Data from 2 independent experiments is shown. Each data point reflects an individual tumor with statistical means shown. **D.** Relative mRNA expression of PI3K *isoforms* $p110\alpha$, β , γ , δ and *Btk* in primary murine macrophages and cultured PDAC clones p53 2.1.1 and Ink4a 2.2. Error bars represent standard errors of the mean. Statistical significance was determined using the student's T test or one-way Anova when analyzing more than two groups, ** $p < 0.01$, *** $p < 0.001$.

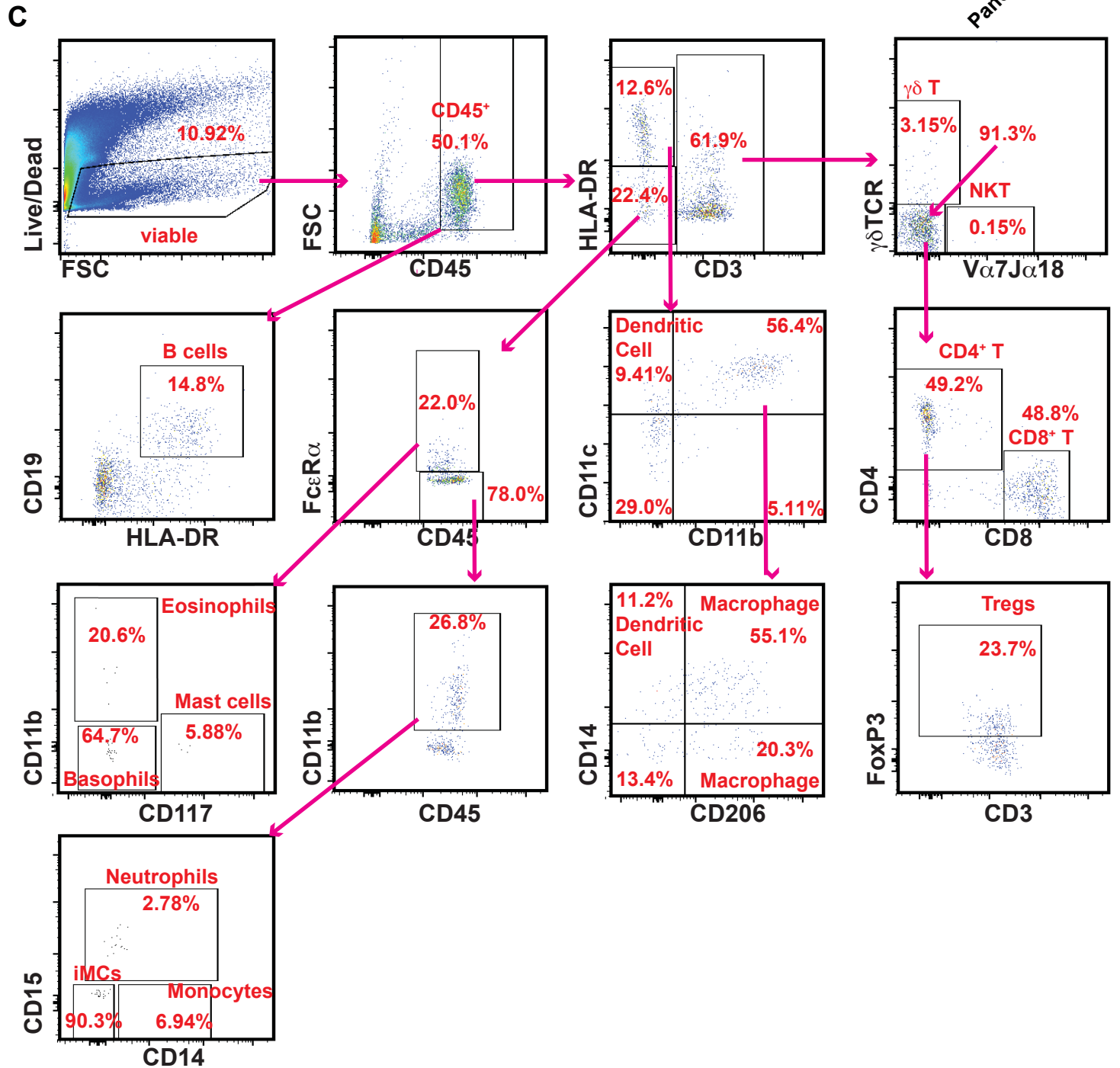
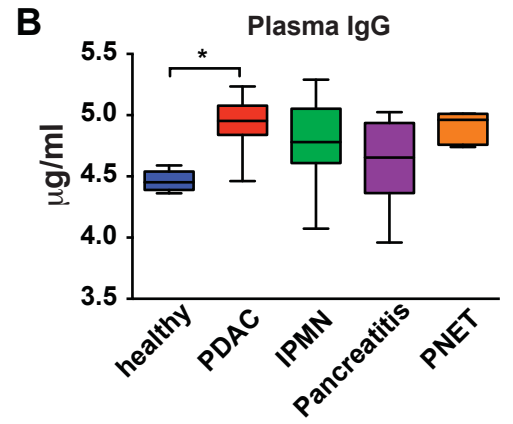
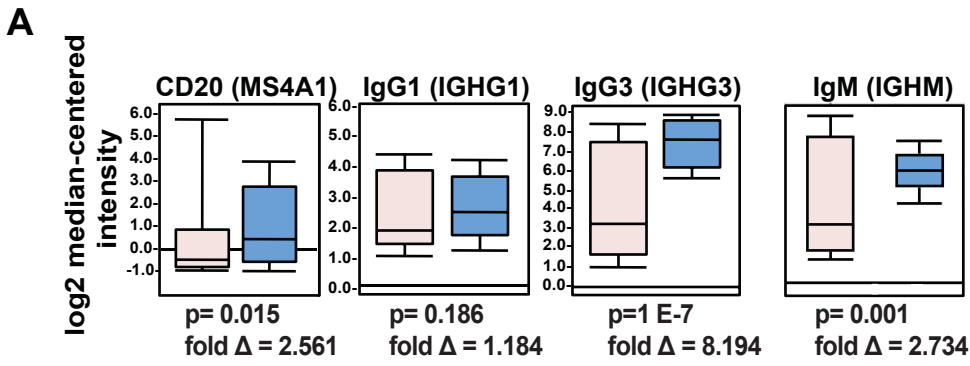
Supplementary Figure S4: Macrophage PI3K γ activates BTK to promote PDAC progression. **A.** Validation of *Btk* siRNA knockdown. **B.** Effect of PCI-32765 on adhesion of SDF-1 α -stimulated primary myeloid cells to endothelial monolayers. **C.** Effect of PCI-32765 on adhesion of IFN γ -stimulated primary B cells to endothelial monolayers. Inset, FACS plot showing purity of isolated B cells. **D.** Effect of PLC γ siRNA on SDF-1 α and IL-1 β -stimulated myeloid cell adhesion to VCAM-1. **E.** Validation of PLC γ siRNA knockdown. **F.** pBTK/BTK Western blotting (cropped gels) in wild type (WT) and p110 γ ^{-/-} IL-4-stimulated primary macrophages. Ratio of pBTK to total BTK is listed under each condition. **G-H.** Effect of PCI-32765 and p110 γ ^{-/-} on IFN γ /LPS (**G**) and IL-4 (**H**) stimulated macrophage gene expression, graphed as mRNA expression relative to basal expression. **I.** Effect of BTK knockdown and embryonic deletion on gene expression of IL-4-polarized murine macrophages. Statistical significance was determined using the student's T test or one-way Anova when analyzing more than two groups, * $p < 0.01$, ** $p < 0.01$, *** $p < 0.001$.

Supplementary Figure S5. BTK and PI3K γ -inhibition decrease PDAC growth. **A.** FACS plot showing purity of isolated Gr1⁺CD11b⁺ cells and B cells used in Figure 5A. **B-C.** Effect of PCI-32765 and vehicle control on (**B**) bone marrow-derived macrophage (BMM) and (**C**) p53 2.1.1 PDAC tumor cell viability. **D.** Effect of TG100-115 and vehicle control on p53 2.1.1 PDAC tumor cell viability. **E.** CBC analysis of murine peripheral blood harvested 2 days post-treatment or 10 days post-treatment with PCI-32765 +/- Gem. Total white blood cells (WBC), polymorphonuclear leukocytes (PMN) and lymphocytes (lympho) are shown from one representative experiment. N = 8 mice/experimental group. **F.** Representative FACS plots of CD19⁺CD220⁺ B cells from p53 2.1.1 tumors grown in WT or p110 γ ^{-/-} animals that were treated with PCI-32765 or vehicle. **G.** Representative photomicrographs showing immunofluorescent staining (green) of CD11b⁺ myeloid cells in mice bearing p53 2.1.1 tumors treated with vehicle (Control), PCI-32765 (PCI), TG100-115 (TG100), gemcitabine (Gem) or combinations thereof. 'Control' indicates vehicle-treated tumor-bearing mice. 'Normal' indicates tumor-naïve pancreata. Scale bar: 100 μ m. **H.** mRNA expression of Arginase 1 in tumor-derived myeloid cells and whole tumors from WT or p110 γ ^{-/-} animals treated with PCI-32765 or vehicle (n=5). Error bars represent standard error of the mean. Statistical significance was determined using the student's T test or one-way Anova when analyzing more than two groups, *** $p < 0.001$.

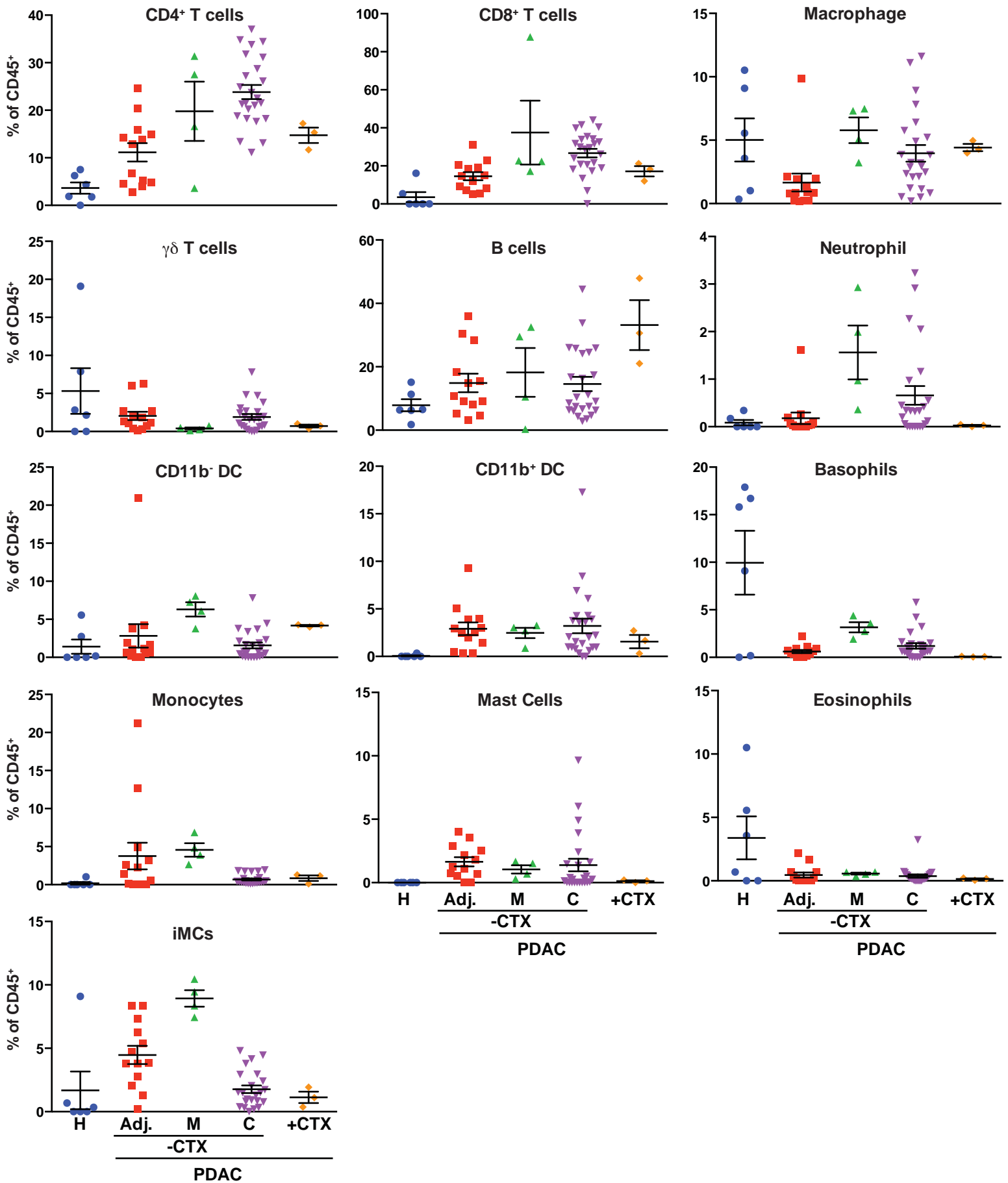
Supplementary Figure S6: BTK inhibition improves gemcitabine response in late-stage PDAC. **A.** Representative photomicrographs of tissue sections from Ink4 2.2-derived PDAC tumors from mice treated as indicated (on top), e.g., vehicle control, PCI-32765, Gem, PCI-32765/Gem, and stained via immunodetection of CD45, Gomori trichrome, and granzyme B. **B.** FACS analysis of Ink4 2.2 PDAC tumors harvested at day 23 post-implantation and assessed for CD8⁺ T cell effector/memory markers PD-1 and EOMES. Data is displayed as a percentage of CD3⁺CD8⁺ cells. **C.** FACS analysis reflecting single cell suspensions of Ink4 2.2-derived tumors from mice treated with depleting CD8 antibodies as indicated (Fig. 6A). **D.** Toluidine blue staining of Ink 2.2-derived PDAC tumors to reveal mast cells, with higher magnification images revealing degranulation (right). Graphs indicate quantitation of total mast cells (left) and percentage of mast cells evidencing a degranulation phenotype as indicated by pericellular granules in the treatment groups shown. Error bars represent standard error of the mean. Statistical significance was determined using the student's T test or one-way Anova when analyzing more than two groups, ns: not statistically significant.

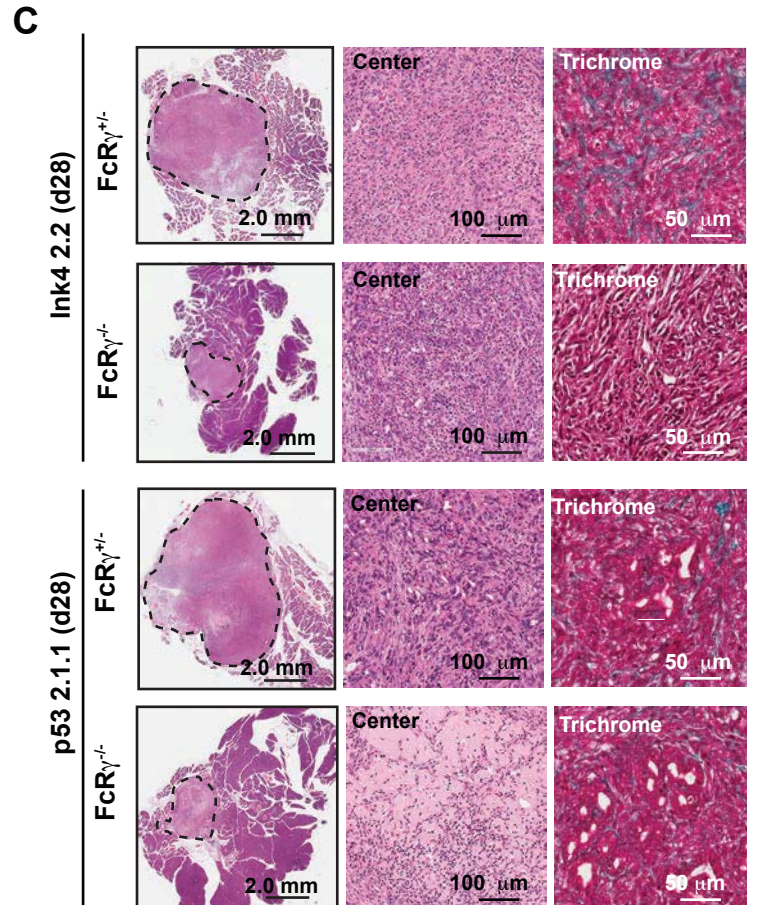
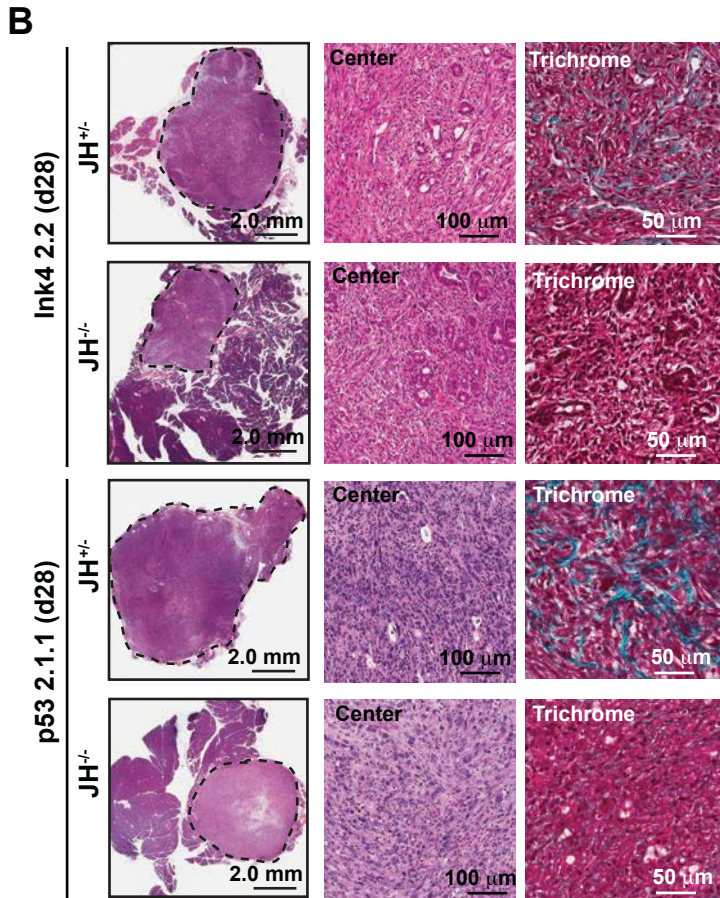
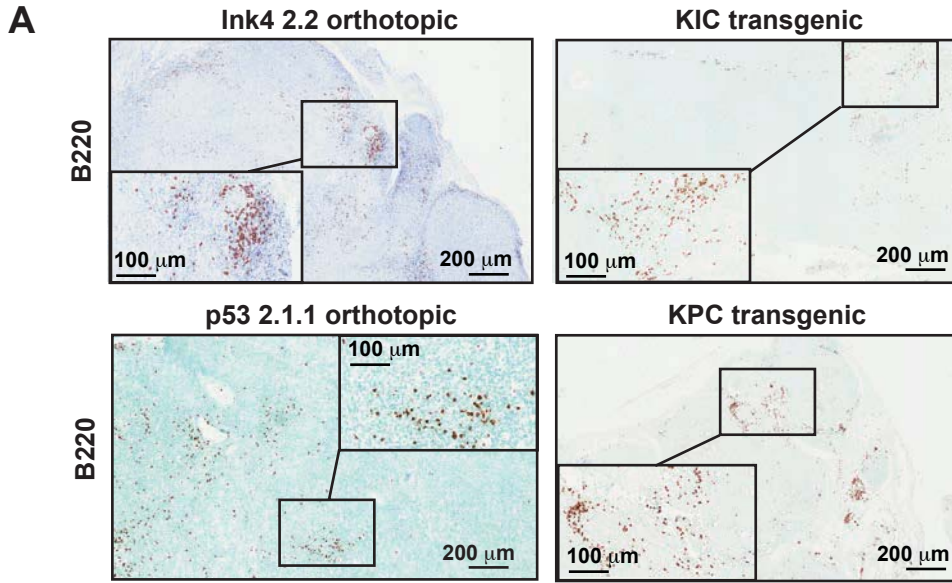
REFERENCES

1. Ruffell B, Au A, Rugo HS, Esserman LJ, Hwang ES, Coussens LM. Leukocyte composition of human breast cancer. *Proc Natl Acad Sci U S A.* 2012;109:2796-801.
2. Glass G, Papin JA, Mandell JW. SIMPLE: a sequential immunoperoxidase labeling and erasing method. *J Histochem Cytochem.* 2009;57:899-905.
3. Stack EC, Wang C, Roman KA, Hoyt CC. Multiplexed immunohistochemistry, imaging, and quantitation: a review, with an assessment of Tyramide signal amplification, multispectral imaging and multiplex analysis. *Methods.* 2014;70:46-58.
4. Affara NI, Ruffell B, Medler TR, Gunderson AJ, Johansson M, Bornstein S, et al. B cells regulate macrophage phenotype and response to chemotherapy in squamous carcinomas. *Cancer Cell.* 2014;25:809-21.
5. Bonecchi R, Sozzani S, Stine JT, Luini W, D'Amico G, Allavena P, et al. Divergent effects of interleukin-4 and interferon-gamma on macrophage-derived chemokine production: an amplification circuit of polarized T helper 2 responses. *Blood.* 1998;92:2668-71.



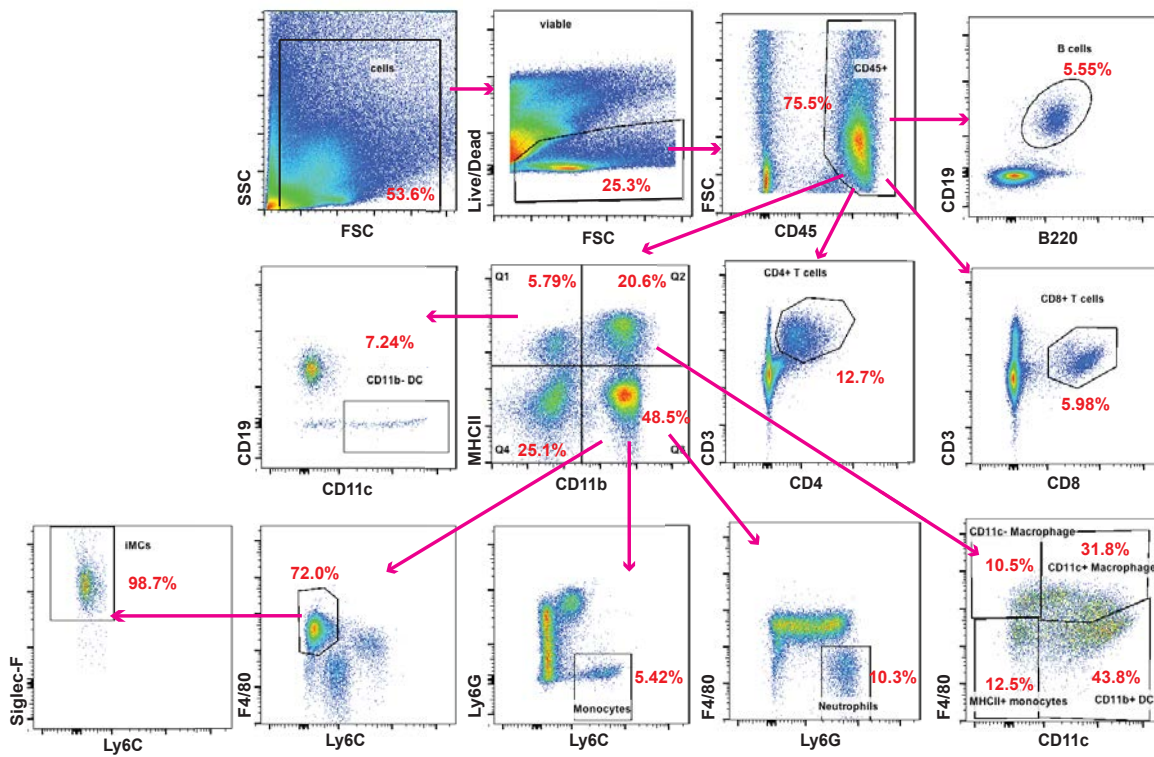
D



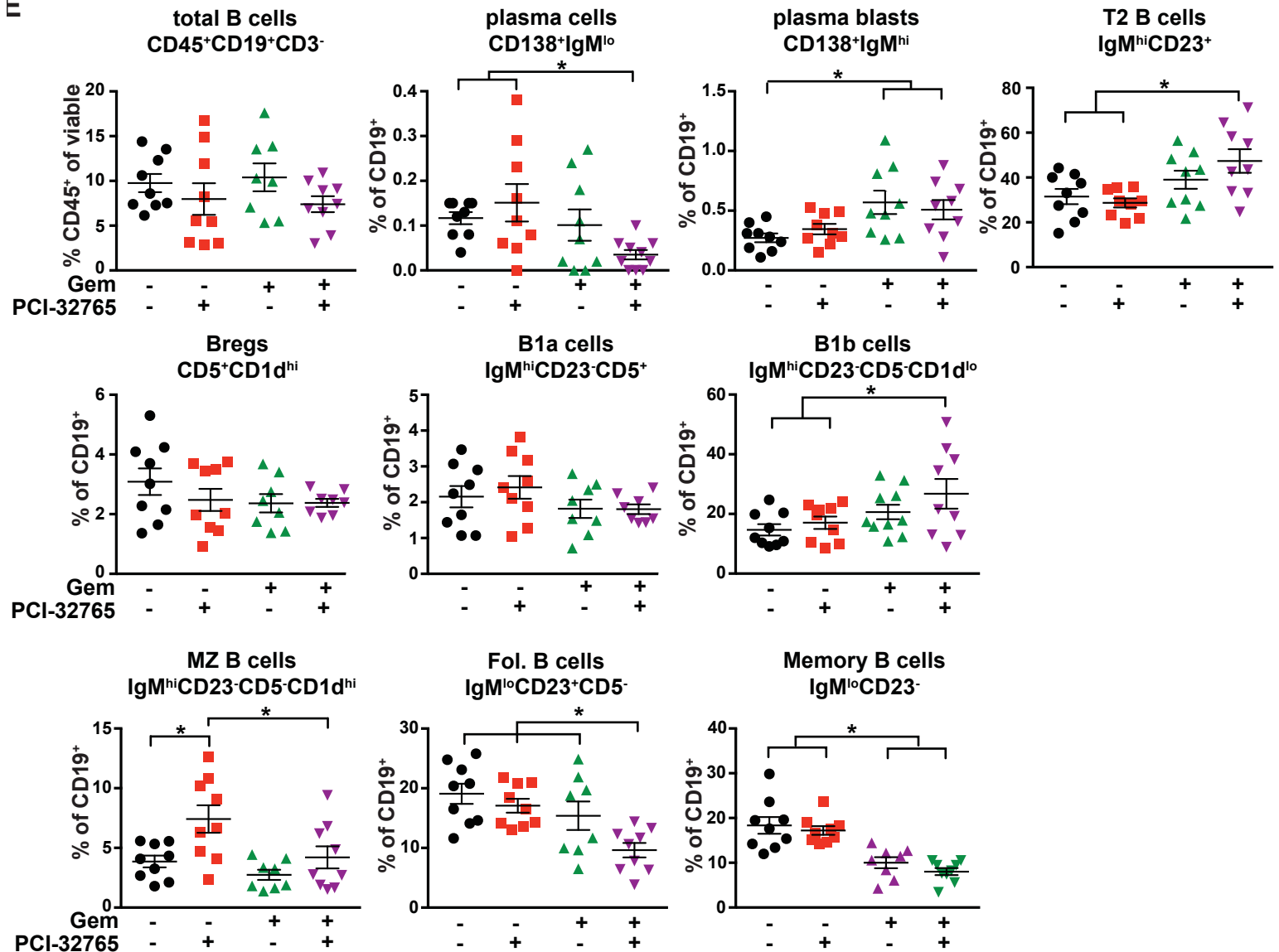


D

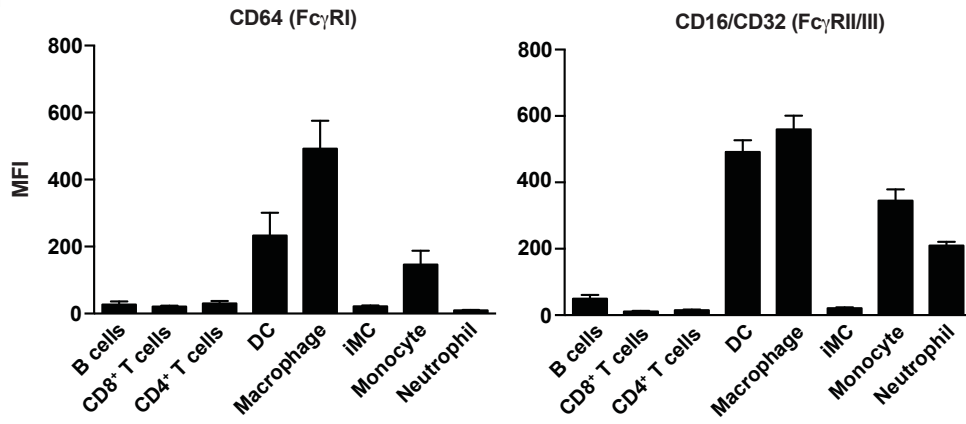
Supplementary Fig. S2D-E



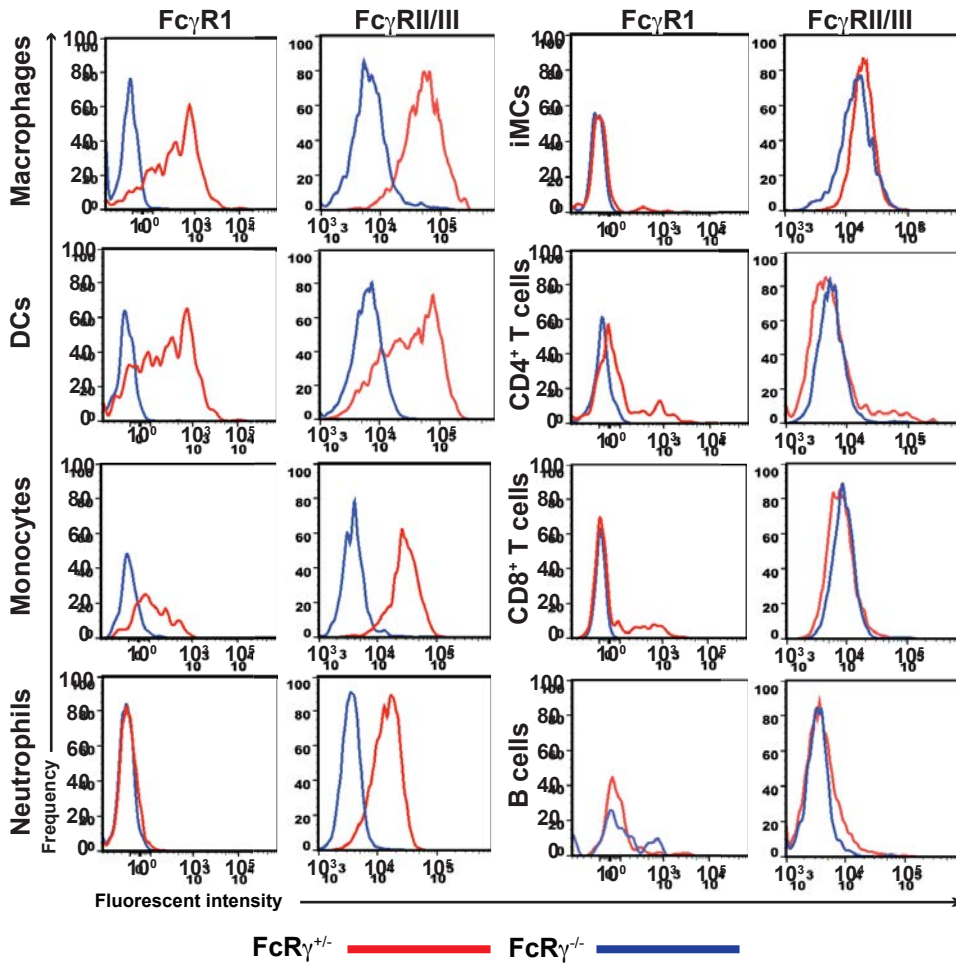
E



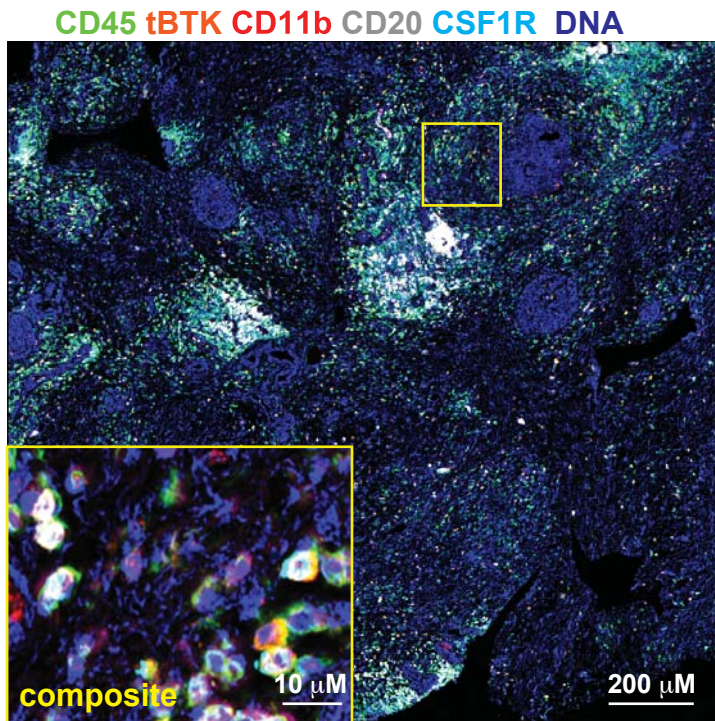
F



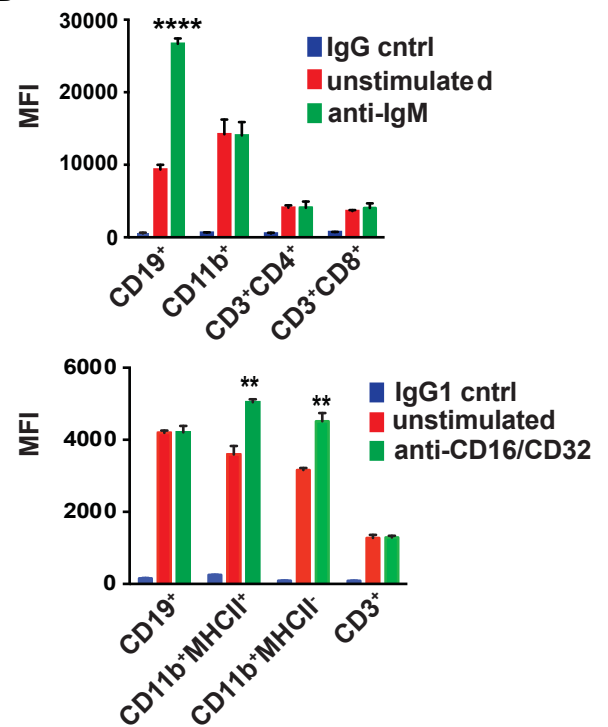
G



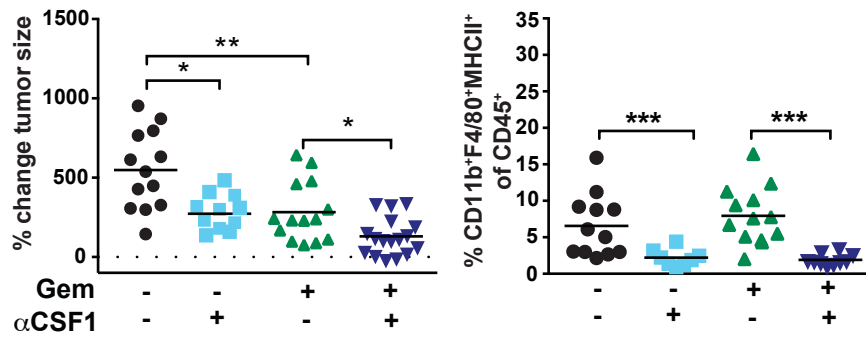
A



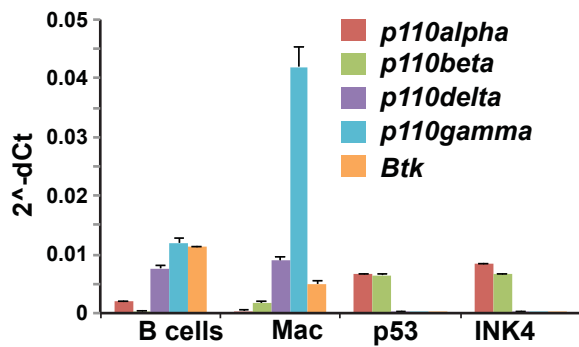
B

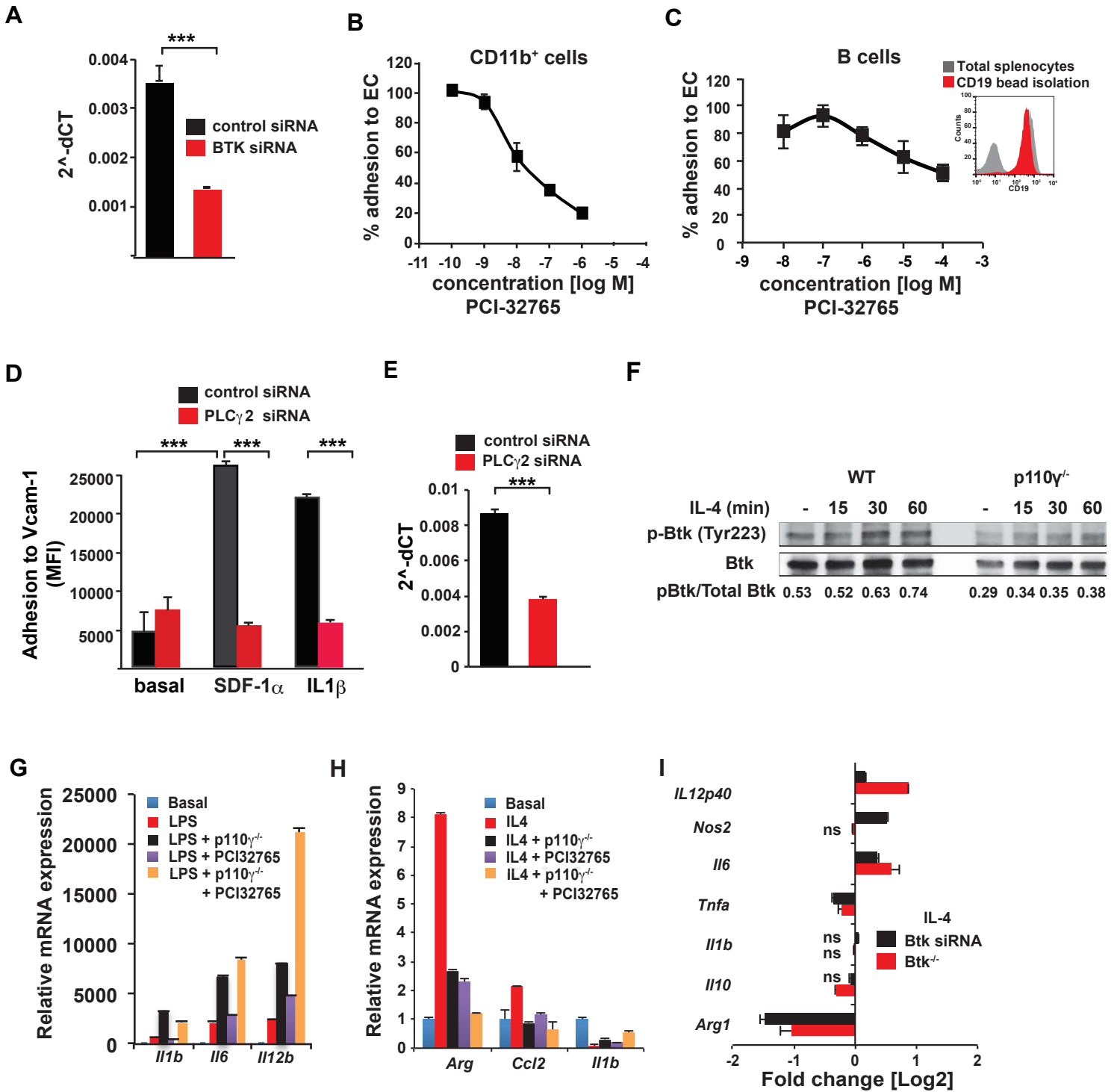


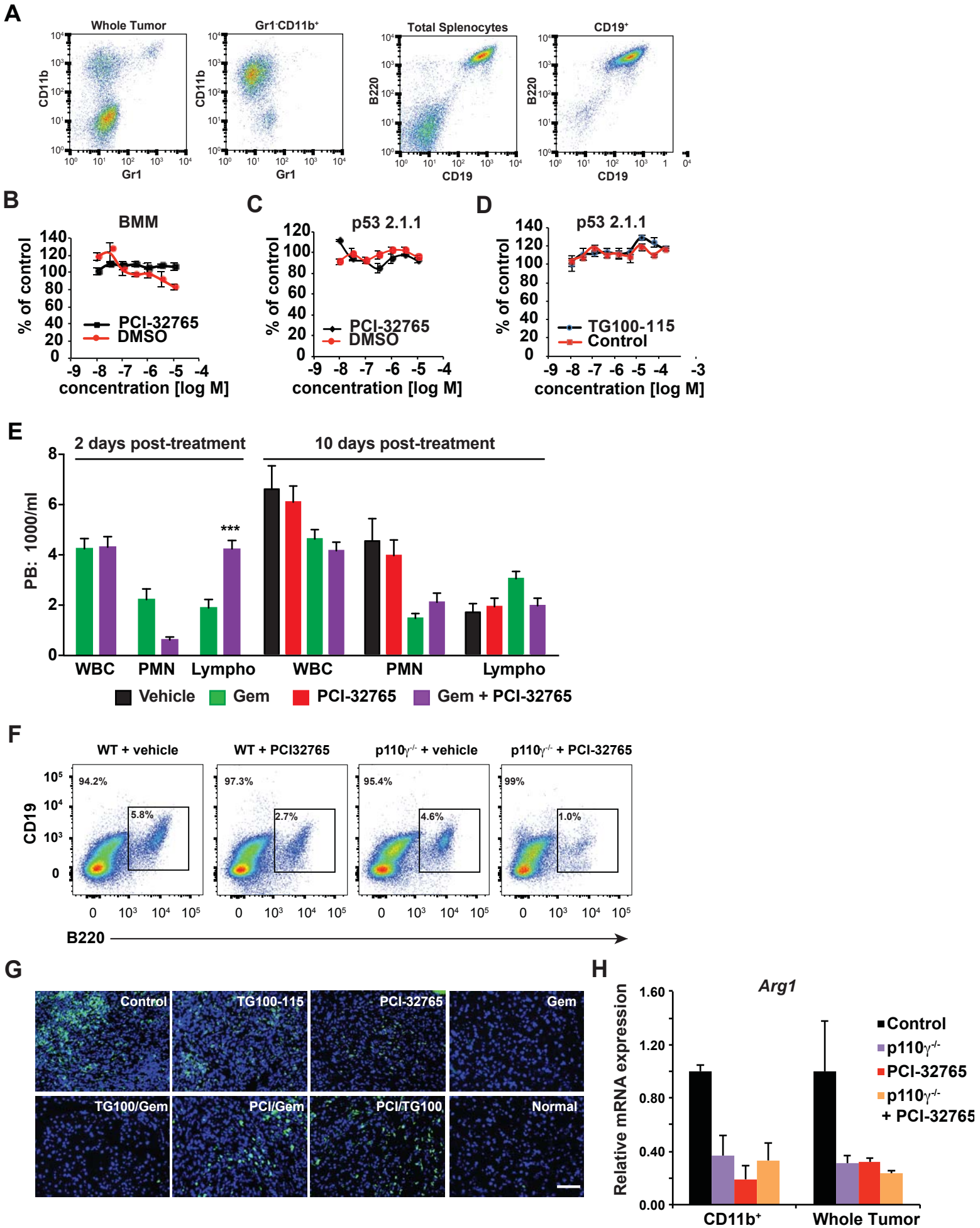
C



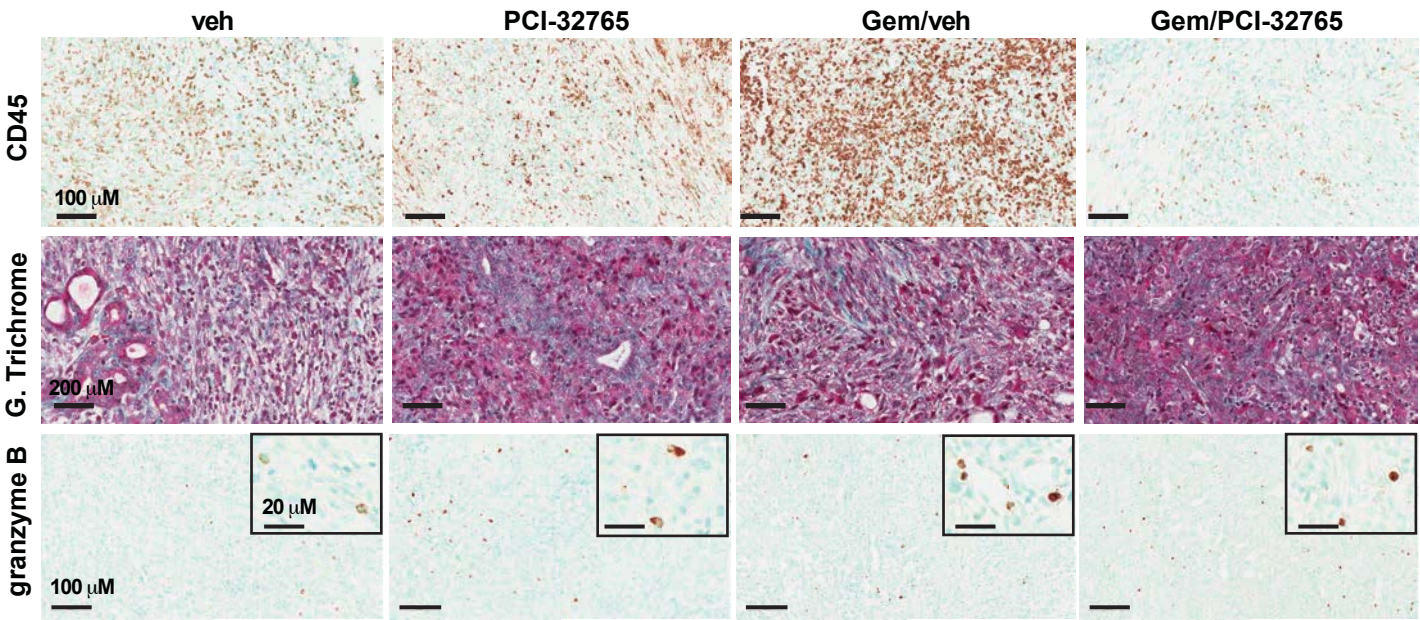
D



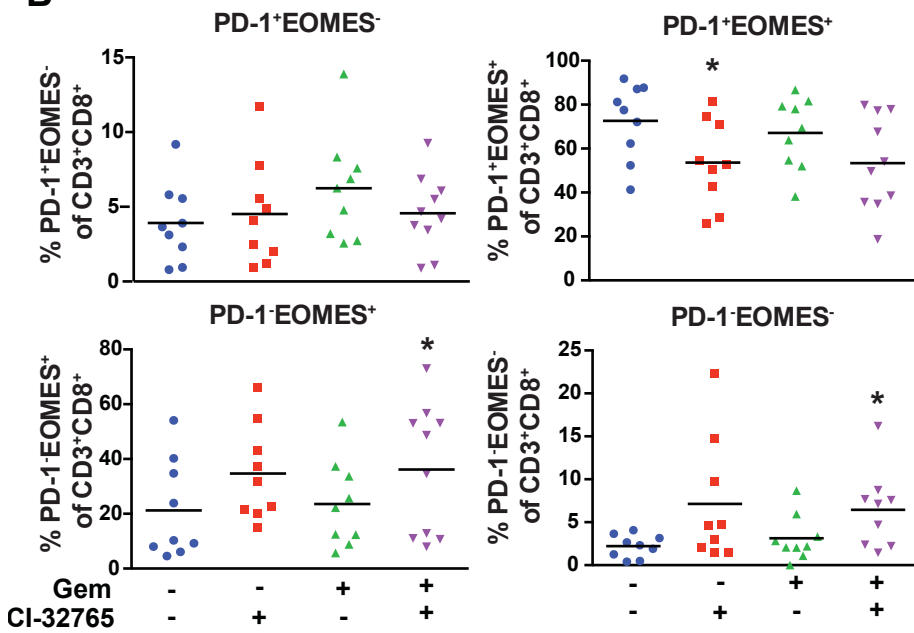




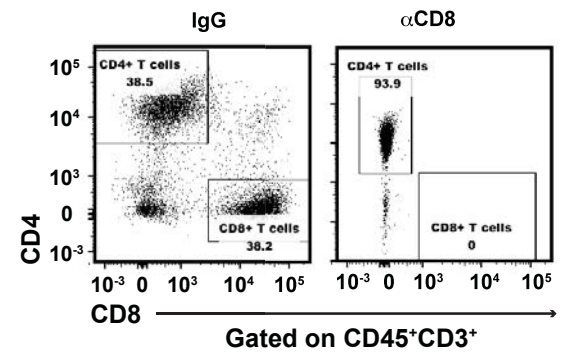
A



B



C



D

